Request for Irradiation of Lead Tungstate Crystals with Hadrons

M.Huhtinen, P.Lecomte, D.Luckey, F.Nessi-Tedaldi

Introduction

The Compact Muon Solenoid (**CMS**) designed for the CERN-LHC collider is a general purpose detector able to run at the highest LHC luminosity. The CMS collaboration, which groups 1800 scientists from 150 institutes in 32 countries, has designed and is presently building the 21.6m long and 14.6m high detector weighting 12 500 ton which must be installed by early 2005. The apparatus consists in a 4T supraconductive solenoid surrounded by muon detectors and containing the tracker as well as calorimeters; barrel detectors are completed by corresponding end caps. The subdetectors must withstand a difficult environment: the tracker and calorimeters operate in a 4T field, there will be only 25ns between beam crossings and around 20 interactions per crossing at full luminosity; correspondingly good time and space resolution are thus essential and must be maintained in the presence of high radiation levels. The required operating lifetime of the subdetectors is over ten years with few possibilities of access for maintenance[1].

The Electromagnetic Calorimeter (**ECAL**) contains 82 728 $PbWO_4$ crystals weighting in total 92.6 tons[2]. The ECAL is totally active to obtain the best possible energy resolution; it is as compact as possible to minimize the magnet size. Our reasons for using 23cm long lead tungstate crystals (Endcaps: 22cm crystals) can be understood by comparing the alternatives, as summarized in the following table:

	BGO	**BaF_2**	**CeF_3**	**$PbWO_4$**
ρ [g/cm^3]	7.13	4.88	6.16	8.28
λ_r [cm]	1.12	2.06	1.68	0.89
λ_i [cm]	21.8	29.9	26.2	22.4
M_r [cm]	2.33	3.39	2.63	2.19
n	2.15	1.49	1.62	2.3
λ_{max} [nm]	480	210/310	300/340	440
T.coef [%/ C]	-1.6	-2/0	0.14	-2
Relative light yield	18	20/4	8	1.3
τ [ns]	60/300	0.9/630	8/25	**>95% of the light in 100ns**

The crystals look like very high density glass, insensitive to air and humidity, relatively brittle; they will be irradiated at doserates of 0.15-0.3Gy/h in the barrel ECAL, at up to 15Gy/h in the endcaps near η=3; detailed simulation have been carried out by one of us[3]. To summarize briefly his note:

*"Assumptions: L=10^{34} cm^{-2}s^{-1}, thus 8*10^8 pp events/second. Luminosity decaying during fill, at ~20% after 20 hours. In 10 years 500 fb^{-1} = 5*10^7 seconds at L=10^{34} cm^{-2}s^{-1}. Two times more hadrons than em interacting particles are expected, carrying in average per event 3 times more energy than em particles. The electromagnetic dose rate profile in EE crystals is quite flat (factor 5 between minimum and maximum). The profile is well reproduced by 400 MeV/c charged pions. Tests with hadrons on crystals have been performed so far up to an integrated dose of only 5.5 Gy. about 10000 less than the purely hadronic dose in the EE at eta=2.9 for 500fb^{-1}. Although several tests with neutrons were made up to several 10^{14}, EE crystals should be tested in a high-energy hadron beam up to fluences of about 10^{14}/cm^2."*

Extensive irradiation tests have been performed in the past five years using gamma and electrons to improve the crystals resistance to radiation, but there have been only few irradiation studies with hadrons[3, 4]. Only recently did we receive the first end caps preproduction crystals and we want to subject some of them to the hadron levels they will encounter in the detector.

Justification

We ultimately wish to expose a full size end cap electromagnetic calorimeter $PbWO_4$ crystal to a hadron flux equivalent to that expected for 10 years of LHC operation, to see if there are irreversible effects due to proton displacement damage, which would affect the light yield and the light absorption in the crystal. $PbWO_4$ crystals have been exposed to gamma rays up to 10^5 Gray and some crystals largely recover their initial properties.The end cap crystals will have in addition to gamma flux a large flux of hadrons which could produce different effects. At higher doses, such hadron fluxes are known to cause dimensional changes, destroy crystal structure and change refractive index. Such effects are observed in zircons at very high doses[7]. The lifetime dose will allow the assessment of potential problems. Such an exposure has been recommended by M.Huhtinen who has irradiated $PbWO_4$ with pions at PSI[3,9]. Talks have been presented to CMS in March and July 2002 and the proposal have been approved by the collaboration.

Objectives of this irradiation

The parameters we want to measure are the crystal light yield and transmission before and after irradiation, with long term monitoring for possible recovery (It would be highly desirable to monitor these parameters also during irradiation[5], but this is too complex to be considered at that stage); we thus hope to separate damages affecting the transmission from those affecting the scintillation mechanism. As a byproduct, we will validate the simulation of the activation level and products.

Procedure

Because we will create a radioactive object we cannot easily handle and measure, we plan to make measurements in steps. To minimize the amount of irradiated material and to protect against errors, pieces cut out of whole crystals will be used for all but the last step, each piece being about 10% of the total crystal weight.

- ***STEP 1:*** *Using only a 5mn proton irradiation, we have compared the activation levels from protons irradiation with the simulation to confirm the latter. (Dave's plot). Using the Cern Ge detector, we also obtained a preliminary identification of the main nuclides produced[8].*
- ***STEP 2:*** *We are building an irradiation holder and carriage container for the full size crystal and will check its mechanical compatibility with the irradiation facility as well as with the light yield and transmission test benches.*
- ***STEP 3:*** *We want to compare the activation levels, decay rate and spectra (this using the CERN Ge detector), both from neutrons and protons irradiations, with the simulations. The irradiation levels can be very low to allow quick transfer to the Ge detector. This will be done using the standard Irrad 1 transfer container.*
- ***STEP 4:*** *Mid August, Irradiate a small crystal of $19\times30\times30$ mm^3 (140g) at full proton dose (10^{14} p/cm^2) in irradiation holder (aluminum tube $40\times40\times230$ mm^3, 3mm wall thickness, approximately 300g); cool at Irrad 1 at least till mid September; transfer to carriage container, test of transfer method. Transfer to our laboratory for measurements; the sample will be stored in a lead shield on the cosmics bench and occasionally transferred to the transmission bench for 10mn measurements.*
- ***STEP 5:*** *End October, same as step 4, but for a full size crystal (front face $28.6\times28.6mm^2$, rear face $30\times30mm^2$, length 220mm, volume $1889cm^3$, mass 1564g). We expect that the crystal will need 3 months to cool down in Irrad 1 to a level we can safely handle.*

Aside from the difficulties in handling activated materials, there are practical problems with the light yield measurements: $PbWO_4$ is a very low light yield crystal and the signal from ^{60}Co sources usually used for these measurements would be masked by the activation, thus a high energy,

triggerable signal is needed. It is impractical to set up a test beam facility, thus we decided to use cosmic rays which deposit about 30 MeV in the crystal and generate an external trigger through scintillators; a shielding is necessary not only to protect the operator, but also to limit the counting rate in the trigger scintillators. The transmission measurement is simpler because the light levels involved are much higher, but adequate operator and detector protection is still needed.

Procedures (small sample and full size crystal)

We intend to exercise the procedures first with an inactive sample, then with a small sample and finally with the full size crystal). In the irradiation facility, the activity of the sample will be periodically measured with the existing monitoring system and the sample then remotely put back to its storage position on the irradiation shuttle. If necessary, the sample can be transferred to the Aerate 1 storage using existing procedures, but as long as the shuttle remains available, we prefer to keep the sample on it.

Once the sample activity is deemed low enough by TIS, it will be transferred into an non irradiated carrier (an Aluminum tube similar to the irradiation holder). The exact transfer method has yet to be discussed and approved, but we hope that a normal hand-held manipulator will be sufficient.

The sample and carrier will then be deposited with a manipulator into a unshielded, labeled box providing at least 100mm of clearance between any part of the crystal and the outside) and hand carried from the Irradiation facility to our basement laboratory in Bldg.2 (that is approximately a 200m walk across a road and parking lot, down a staircase near the main shop and 50m along a basement corridor). Thus the irradiated samples will remain at all times on the CERN 1 site.

The sample and carrier will be transferred to the spectrophotometer for a 10mn measurement, then installed in a lead shield on the cosmics bench for a 24h-48h measurement; coupling of the crystal/carrier to the photomultiplier will be via an air gap to minimize handling; the carrier will have been preadjusted to define the crystal position relative to the photomultiplier and will just slide in place into a light tight housing which cap can then be closed. Later, there will be occasional transfers to the spectrophotometer for 10mn measurements and back to the lead shield on the cosmics bench. For these 10mn measurements, only one person will be permitted closer than 1m from the spectrophotometer.

Our basement laboratory already houses sources; it displays the corresponding warnings and its access is limited. Irradiated samples disposal will be through CERN services.

Estimation of produced radionuclides and their activities

Both the LHC experiments have estimations of lead and tungsten induced radioactivity. The enclosed note from CMS gives the detail of our estimates[6]. ATLAS also has produced Internal note 12, May 2000. Lead and Tungsten are well known and common beam dump materials. Effective measurements have already been performed[8,9]. STEP 3 of our procedure should confirm and expand this information, although the number of radionuclides produced is so large that it exceeds the capacity of the existing emission lines identification program.

REFERENCES

1. CMS Collaboration, ***Compact Muon Solenoid Technical Proposal***, *CERN/LHCC 94-38, LHCC/P1 (1994),* CERN, Geneva (Switzerland).

2. CMS Collaboration, ***The Electromagnetic Calorimeter Project***, Technical design report, *CERN/LHCC 97-33. CMS TDR 4 (1997),* CERN, Geneva (Switzerland).

3. M.Huhtinen, ***Radiation environment of the Encap ECAL***, in annex

4. M.Huthinen, ***On hadron irradiation of CMS endcap crystals***, DRAFT, in annex

5. F.Nessi, ***Monitored Irradiations of EE2461 at PSI-Eichlabor,*** preliminary results, in annex

6. M.Huthinen, ***Production of long-lived radionuclides in CMS***, CMS note 1998-044, in annex

7. H.D.Holland and D.Gottfried, ***The effect of nuclear radiation on the structure of Zircon***, Acta Cryst. (1955), 8, 291. Paper copy enclosed.

8. Courtesy of Maurice Glaser, Cern: ***Nuclide Identification report***, July 15, 2002. Paper copy enclosed

9. P.A Aarnio et al., ***Gamma-Spectrometry and residual nuclide analysis of pion-irradiated $PbWO_4$ crystals***, Journal of Radioanalytical and Nuclear Chemistry, vol.248, No.2 (2001) 385-393. Paper copy enclosed

Radiation Environment of the Endcap ECAL

Mika Huhtinen

CERN EP/CMM

Luminosities and multiplicities

About 8×10^8 pp-events per second at L=10^{34} cm^{-2}s^{-1}

Luminosity decays fast during fill
• about 20% of initial lumi left after 20 hours •

For long-term integrated values we assume that in 10 years we accumulate 500 fb^{-1}

500 fb^{-1} = 5×10^7 seconds at L=10^{34} cm^{-2}s^{-1}

Particle composition and energy flow towards EE (effects due to magnetic field not considered)

Average values per event and per EE (η=1.6-2.95)		
Particle	**Multiplicity**	**Energy (GeV)**
pion0	3.48	8.33
photon	0.488	1.03
e+e-	0.006	0.007
Total EM	**3.97**	**9.37**
pion+/-	6.28	15.7
K+K-	0.71	2.69
kaon0	0.71	2.74
neutron	0.47	2.12
proton	0.46	1.95
neutral h	0.15	0.731
charged h	0.075	0.355
Total Had.	**8.86**	**25.59**

Neutron (E>100 keV) fluxes in the EE region

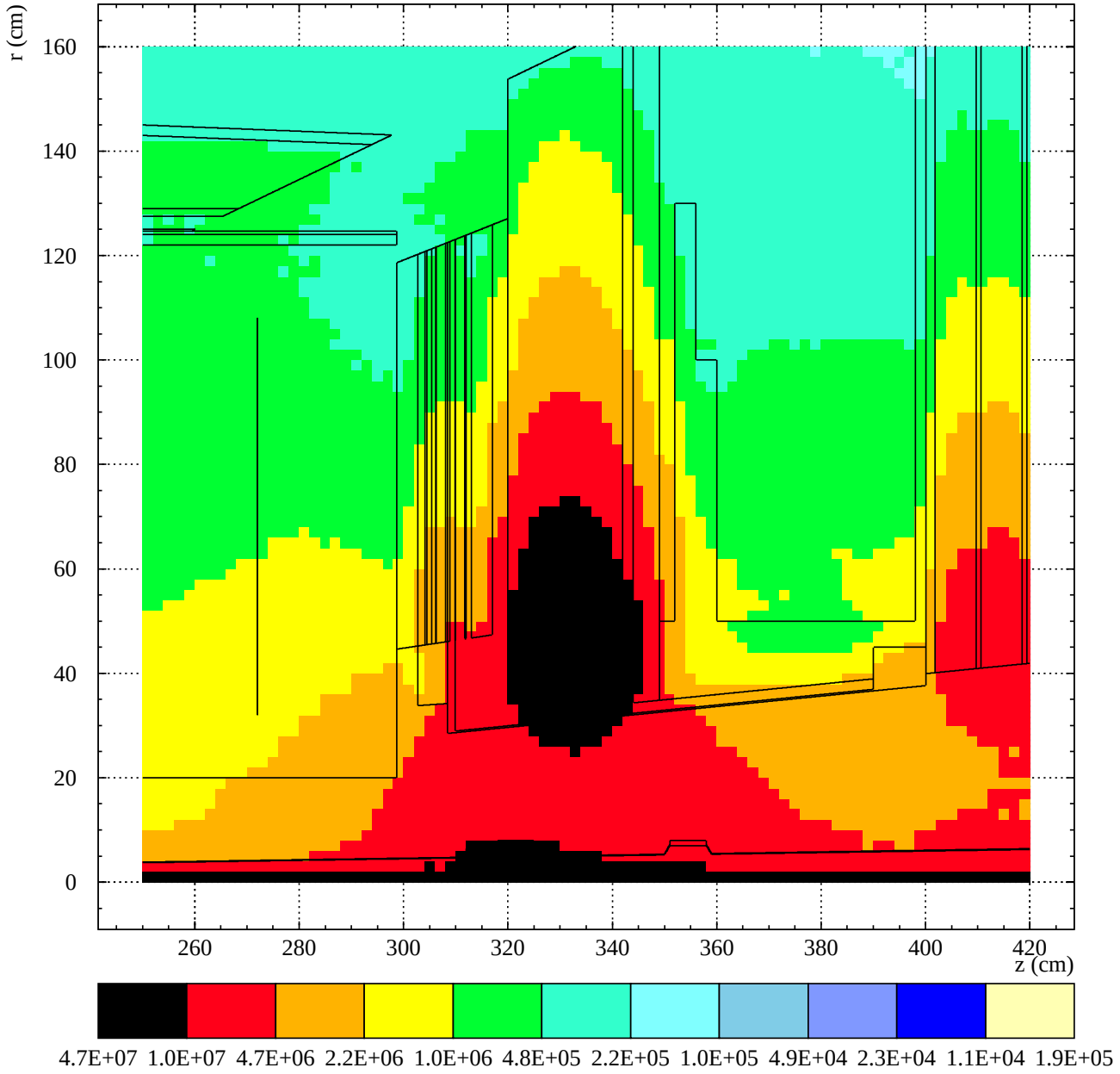

Fluxes in $cm^{-2}s^{-1}$ at $L=10^{34}$

Neutron fluxes E>100 keV contribute to silicon bulk damage

Neutron (E>100 keV) flux profiles in EE

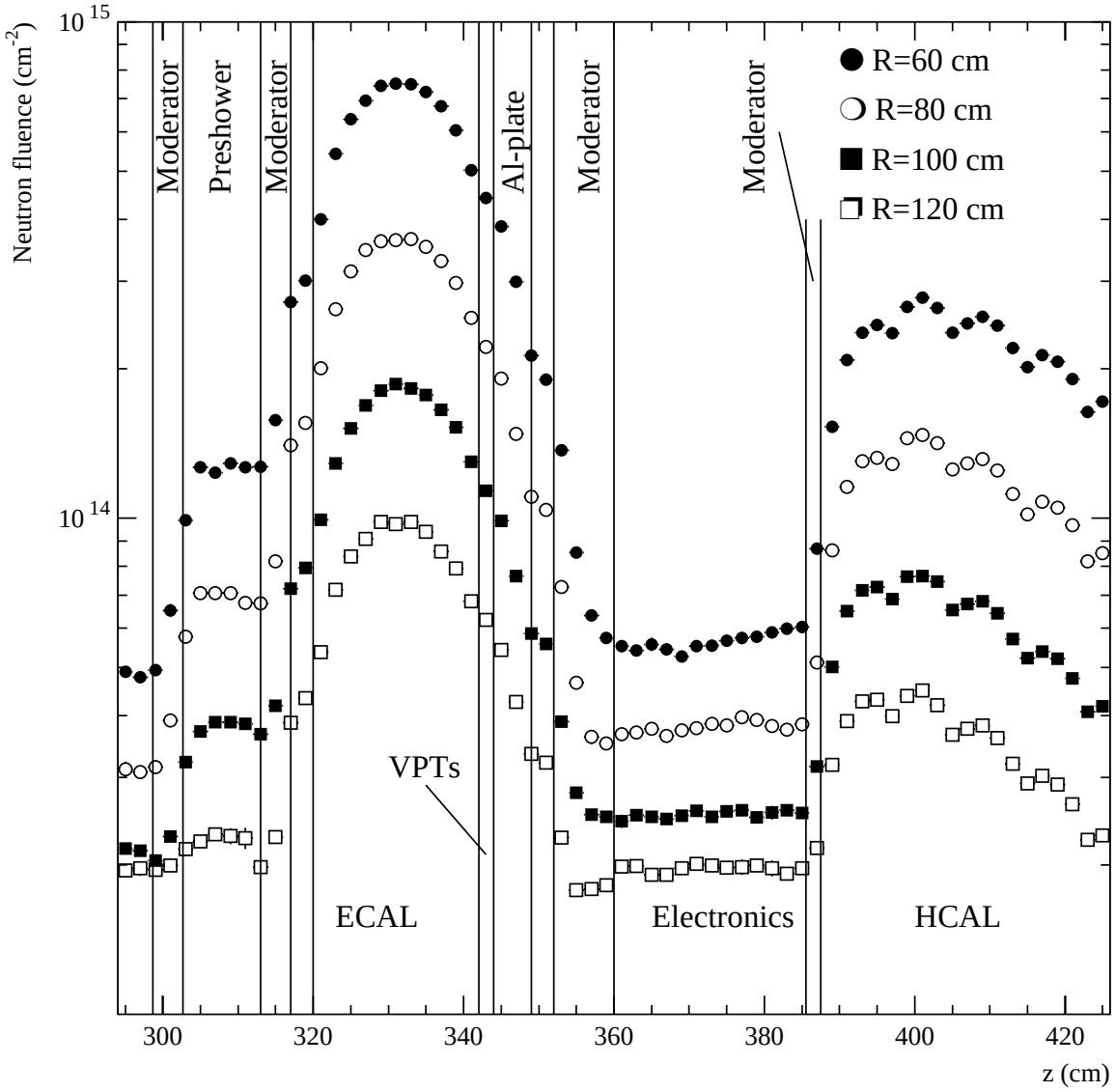

EE crystals are the source of neutrons

Moderators in front of EE protect SE and Tracker

Moderators behind EE optimized to get balanced flux from EE and HE within the electronics space behind EE

Neutron (E>20 MeV) fluxes in the EE region

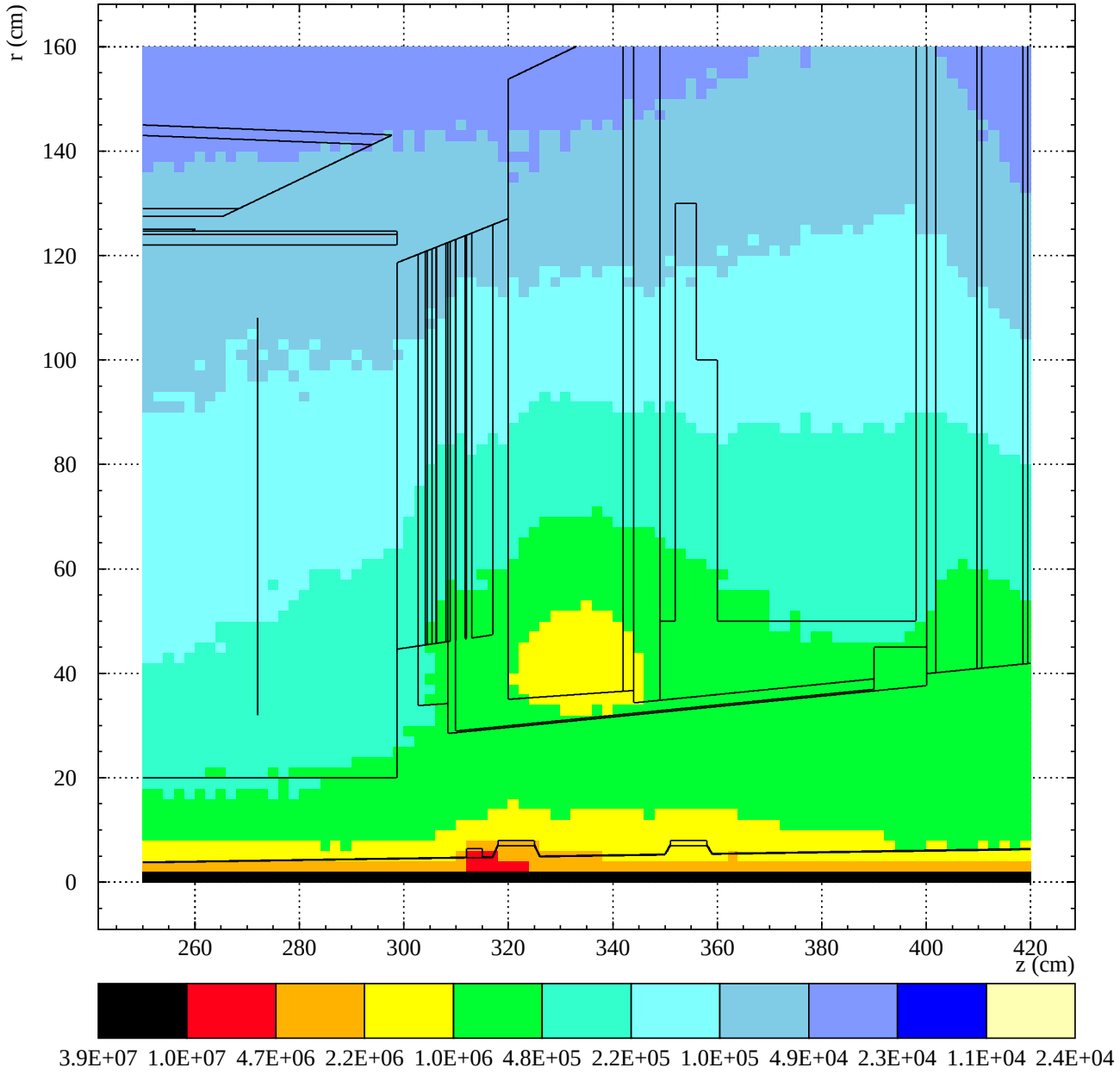

Fluxes in $cm^{-2}s^{-1}$ at $L=10^{34}$

Neutron fluxes E>20 MeV can cause Single Event Upsets in electronics

Charged hadron fluxes in the EE region

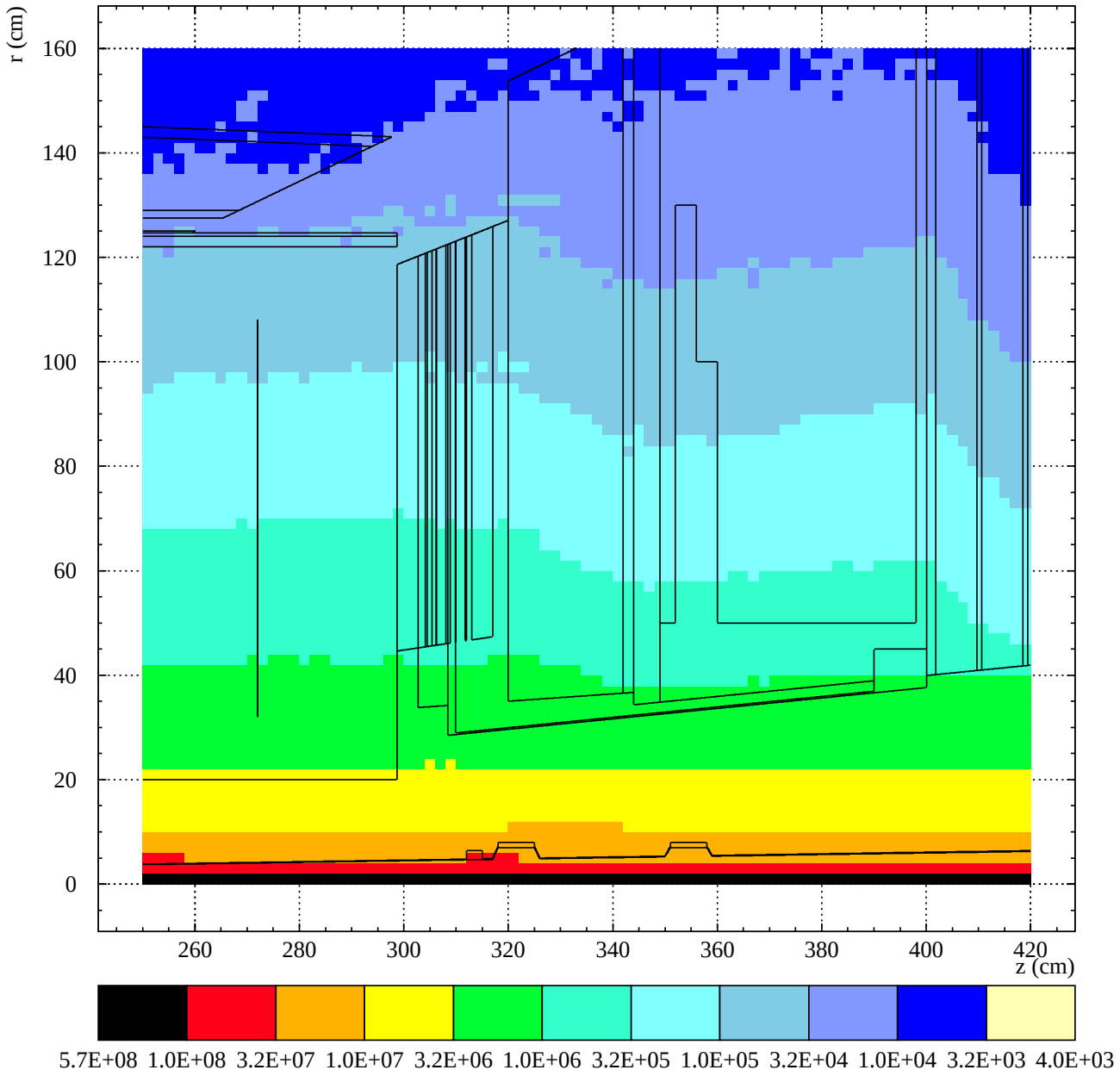

Fluxes in $cm^{-2}s^{-1}$ at $L=10^{34}$

Charged hadrons contribute to radiation dose, silicon bulk damage and can cause Single Event Upsets in electronics

Muon fluxes in the EE region

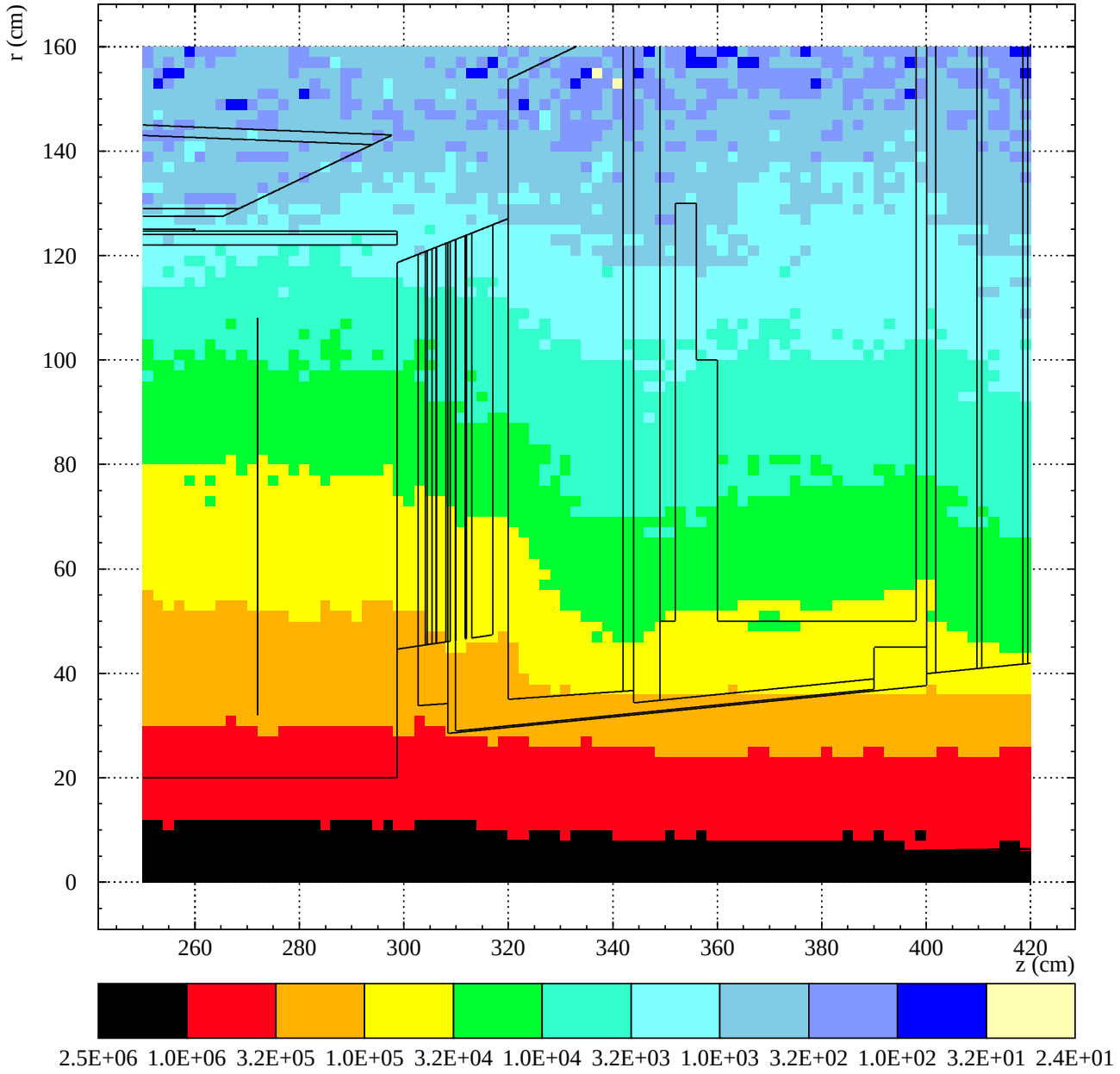

Fluxes in $cm^{-2}s^{-1}$ at $L=10^{34}$

Muons contribute to radiation dose, but are negligible in the EE

Electron (and e^+) fluxes in the EE region

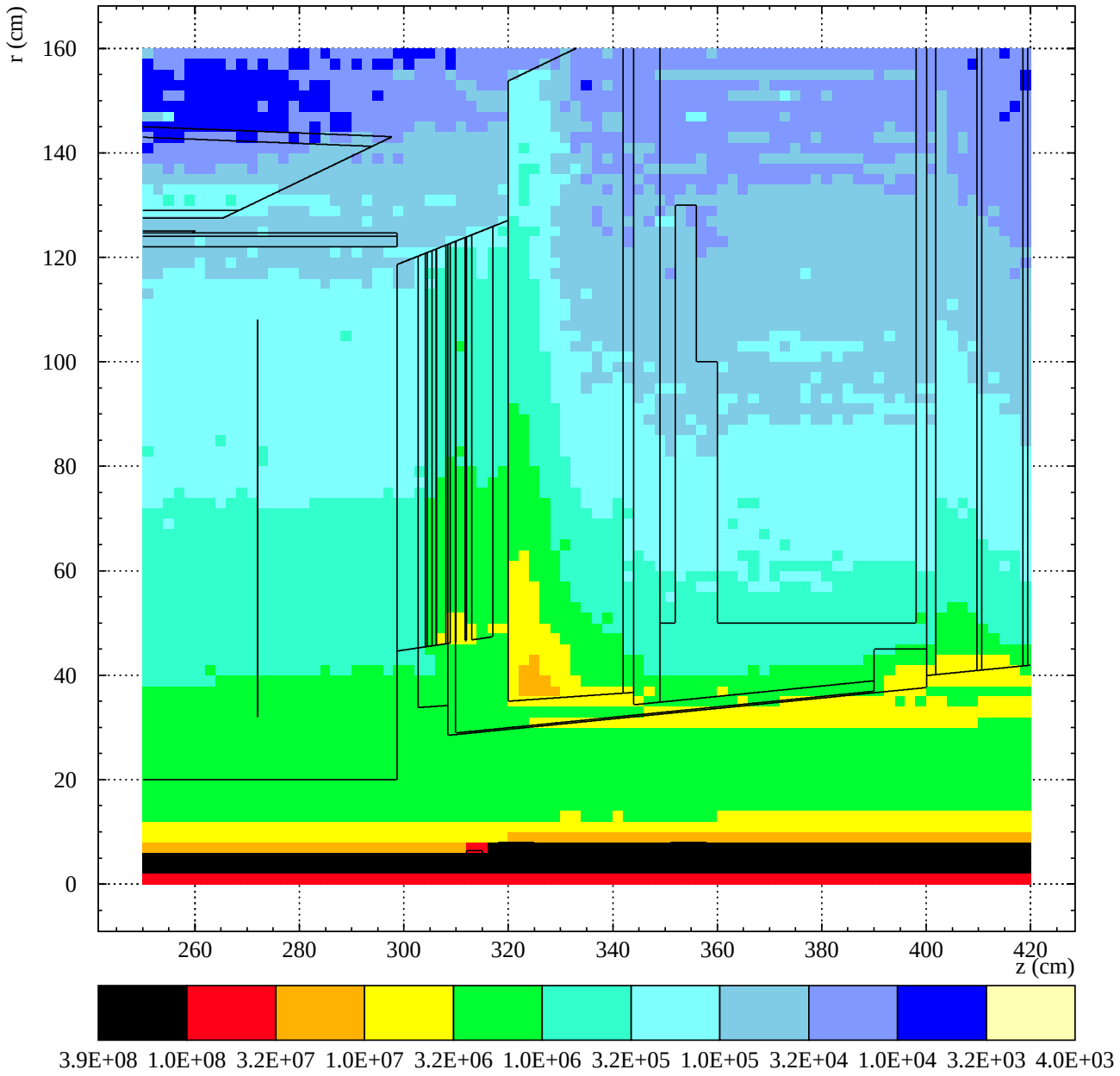

Fluxes in $cm^{-2}s^{-1}$ at $L=10^{34}$

Electrons contribute to the radiation dose

Dose in the EE region

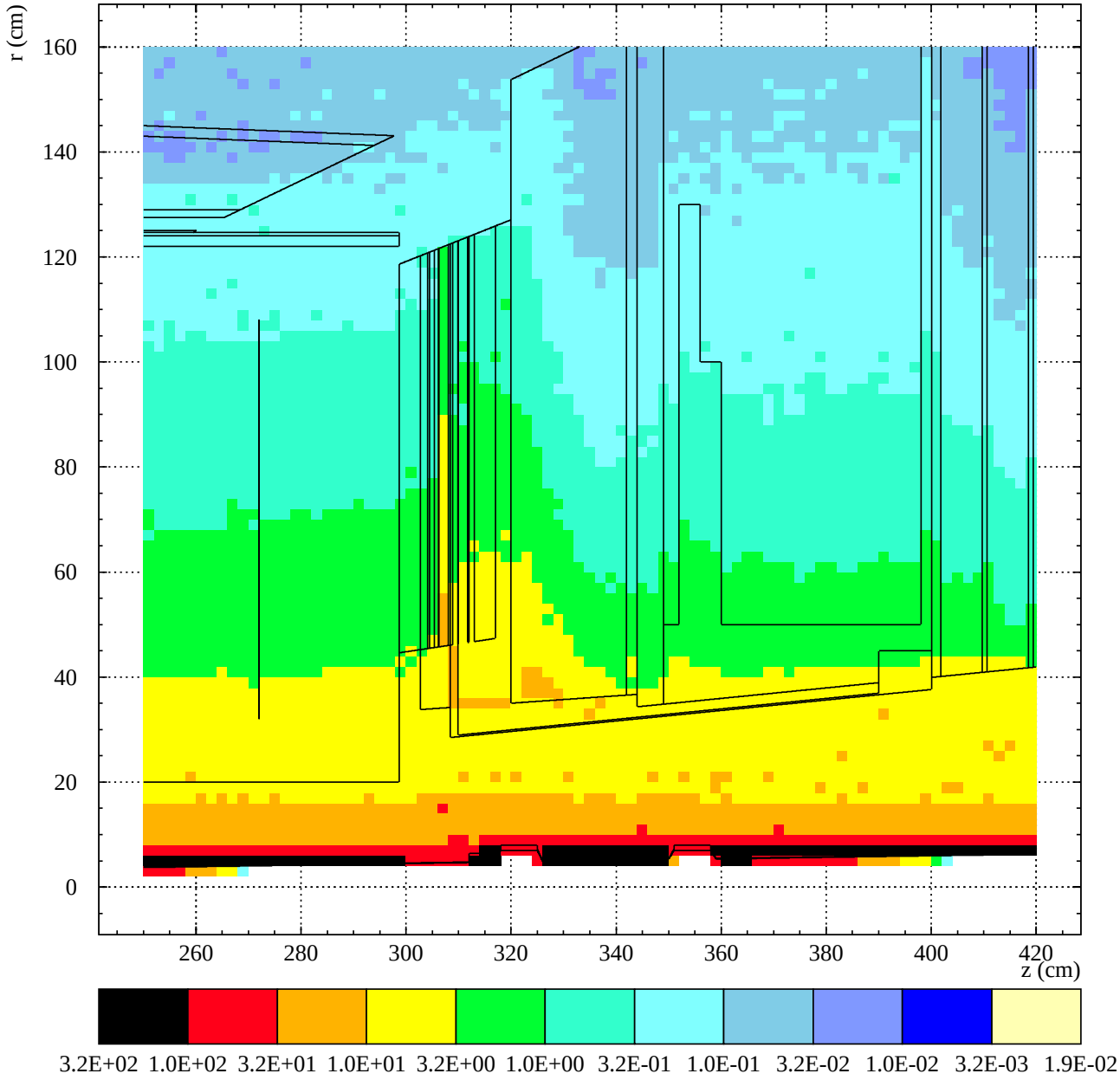

Radiation dose in Gy/h at L=10^{34}

Radiation dose causes damage in CMOS electronics, plastics and the EE Crystals

Dose profiles in ECAL Crystals

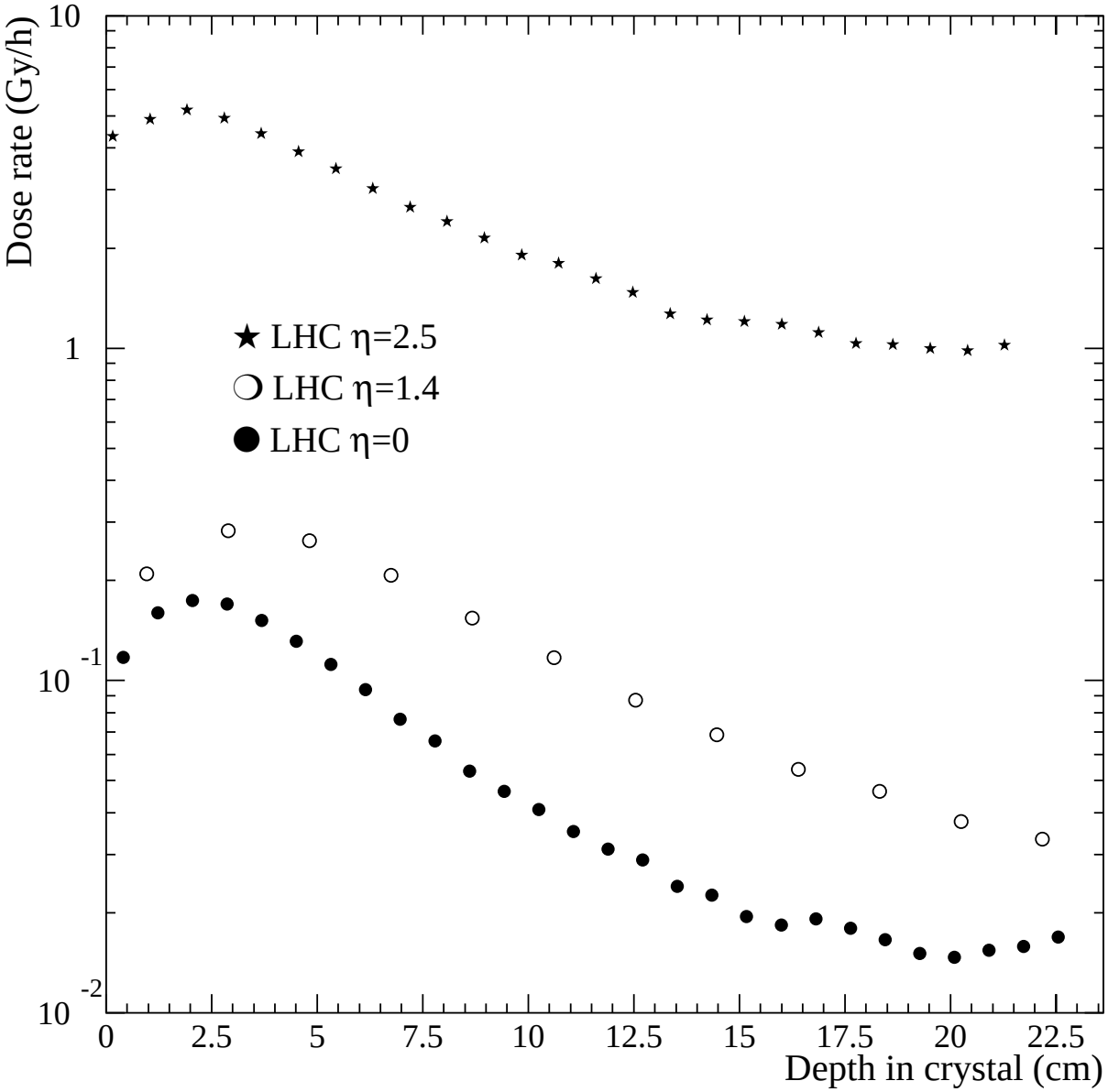

Significantly higher dose rate in EE than in EB

Dose profile quite flat in EE (factor 5 between min and max)

EM and Hadronic dose in ECAL Crystals

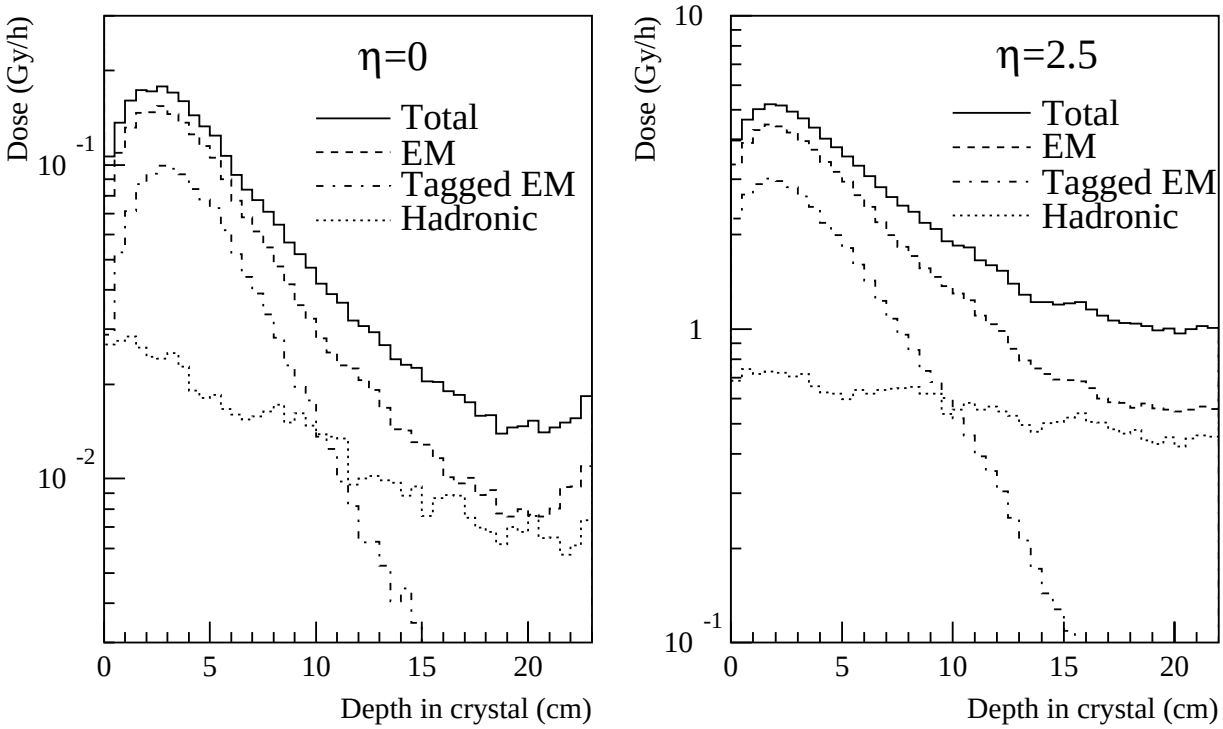

Hadronic: **Energy deposition due to dE/dx of charged hadrons**
EM: **Energy deposition by electrons and positrons**
Tagged EM: **Energy deposition due to EM-particle at IP**

The non-tagged EM-deposition is due to decays, cascading and photons from nuclear de-excitation and neutron capture.

Comparison with γ front-irradiations

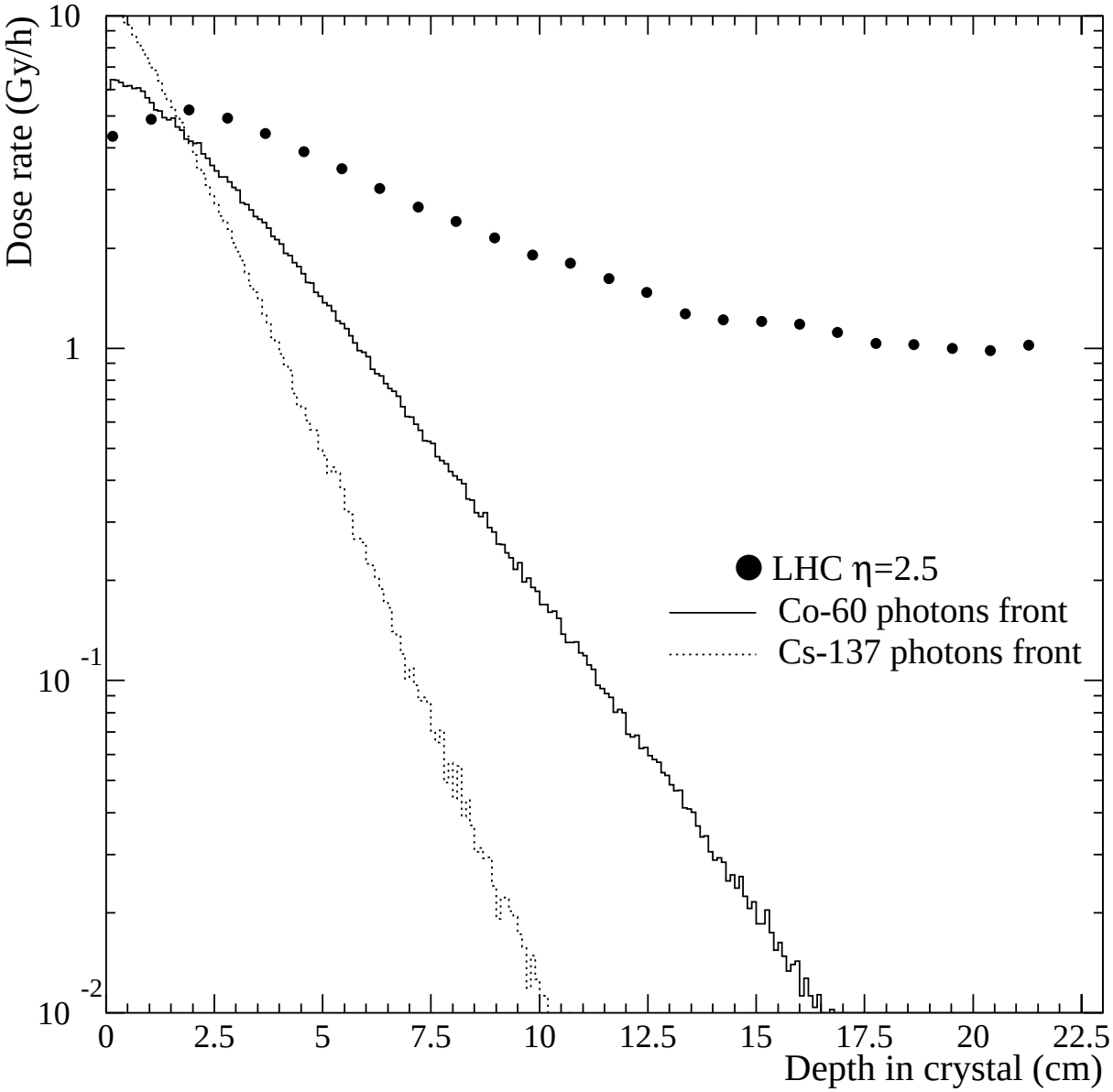

LHC profile not at all reproduced

Comparison with pion front-irradiations

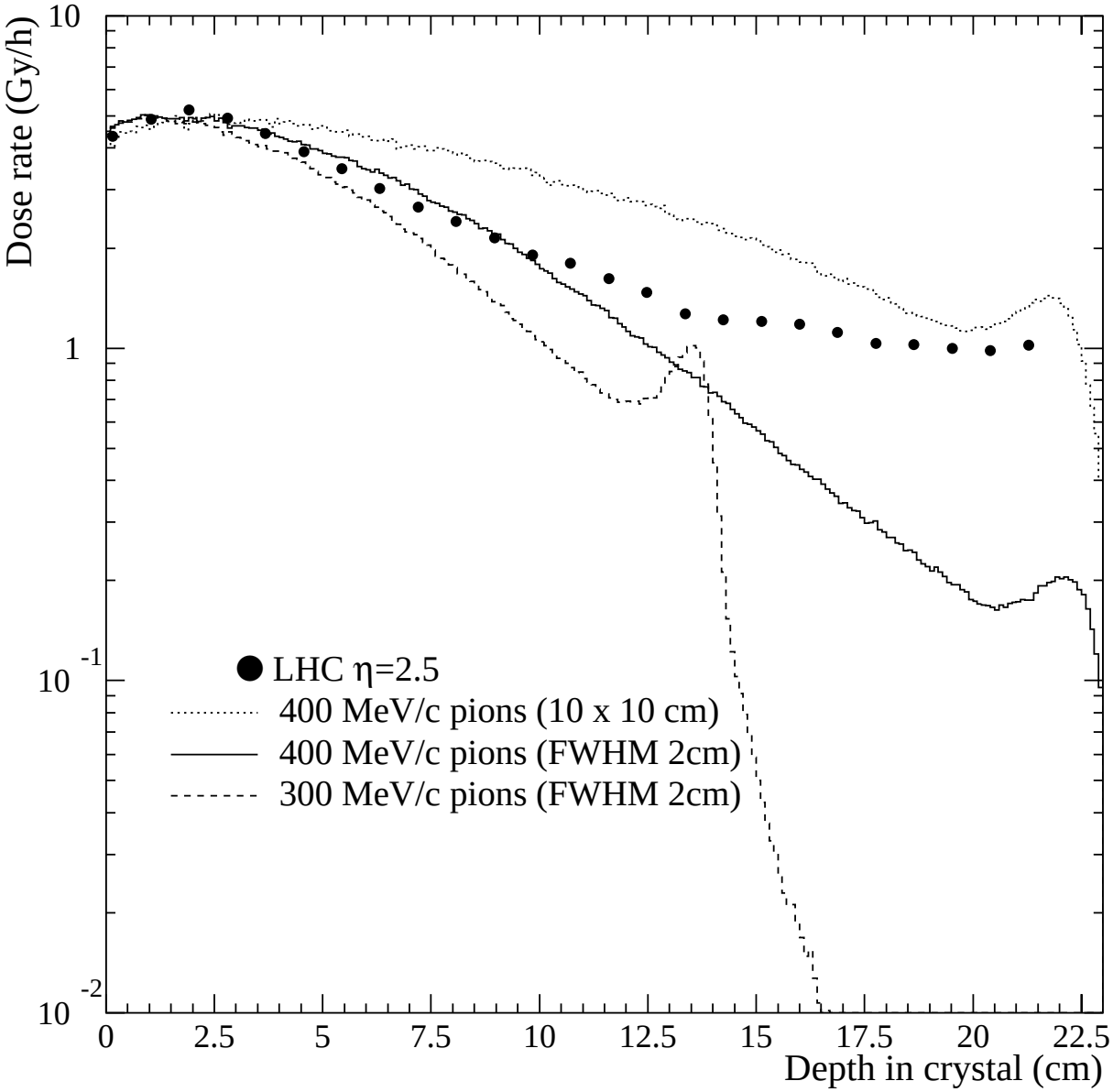

LHC profile rather well reproduced for 400 MeV/c pions

Pions below 400 MeV/c stop within the crystals

Possibility of hadron damage ?

Pending question since 1995...

Partial answer in 1998 with pion irradiations (CMS NOTE 1998/069):

No additional (hadron) damage observed, but

Integrated dose of only 5.5 Gy
About 10000 times (!!!) less than purely hadronic dose in EE at η=2.9 for 500 fb^{-1}.

⇓

This test cannot exclude possible cumulative hadron damage

Existing tests with (reactor) neutrons are not conclusive either, because damage mechanisms of reactor neutrons and high-energy hadrons might be very different.

⇓

EE Crystals should be tested in a high-energy <u>hadron beam</u> up to sufficiently high fluences of about 10^{14} cm^{-2}.

Conclusions

Radiation environment of EE at high-η comparable to CMS Pixel

Quantity	Hadr. E>100 keV	Hadr. E>20 MeV	Dose (Gy)
Pixel R=11 cm	4.6×10^{14}	4.4×10^{14}	1.9×10^{5}
EE Xtal R=40 cm	1.2×10^{15}	1.4×10^{14}	1.6×10^{5}
EE Electronics R=60 cm	5.6×10^{13}	3.8×10^{13}	1.5×10^{4}

Although protected, EE electronics is still in high-radiation area.

Need to consider dose and bulk damage effects, but also SEU !!!

EE crystals exposed to very high dose

...but...

Crystal degradation due to (photon) dose seems understood

Possibility of hadron damage at EE fluences not yet clarified

CMS IN 2002/DRAFT

CMS Internal Note

June 28, 2002

On hadron irradiation of CMS Endcap Crystals

Mika Huhtinen

CERN, CH-1211 Geneva, Switzerland

Abstract

...for the time being this is only a partial DRAFT...

This note describes the simulations for the dose, flux, star density and induced activity of the proposed Crystal irradiation test at the PS.

1 Introduction

Over the last seven years the radiation hardness of the $PbWO_4$ crystals for the CMS electromagnetic calorimeter has been thoroughly tested with γ-irradiation. However, at CMS the crystals will be also exposed to a non-negligible flux of charged hadrons. For 10 years of operation (500 fb^{-1}) this hadron flux is about 10^{12} cm^{-2} in the barrel and increases up to 10^{14} cm^{-2} towards the η=3 corner of the endcap [1)].

In addition to photons the radiation hardness of the crystals has been tested also with reactor neutrons. Also hadron irradiations have been performed but only to fluxes 3–4 orders of magnitude below the expected endcap values.

Although there is no indication for special hadron induced damage, it cannot be excluded that exposure to fast hadrons might not slowly introduce accumulative damage of a type which cannot be introduced by purely electromagnetic irradiation. Such damage – if it exists – would most likely be related to the nuclear reactions of the fast hadrons with the nuclei in the crystals. These effects would not be seen in γ-irradiations and also not during tests with reactor neutrons, where the nuclear interactions are not violent enough.

The unique feature of energetic hadronic collisions is the production of heavy fragments. In the heavy elements of the crystals (W and Pb) these can even be fission fragments. Thus they can have energies up to about 100 MeV per fragment. The production of these fragments has two consequences, neither of which will be seen in any other kind of irradiation:

1. introduction of very short tracks (few μm) with extremely high dE/dx (up to 1000 times a mip)
2. introduction of lattice defects and impurity atoms in the crystal.

In order to experimentally verify that these defects do not lead to unexpected degradation of the crystals, it has been proposed to do a hadron irradiation test up to the full endcap fluence of 10^{14} cm^{-2}.

2 Irradiation at the PS

A suitable facility to perform such a test is the IRRAD1 zone at the CERN PS, where the desired fluence can be reached in about 10 hours.

It has been decided to keep the test as simple as possible, concentrating only on a measurement of optical transmission and light yield of the irradiated crystal. Even the latter of these two measurements might be problematic due to the induced radioactivity in the crystal.

The beam in the IRRAD1 facility consists of 24 GeV/c proton and is roughly Gaussian with FWHM of 2 cm in both directions.

Full-sized endcap crystals will be used for the test. They have a length of 22 cm and lateral dimensions of 2.6×2.6 cm^2.

3 Simulation of the irradiation

The simulations for the irradiation have been performed with the FLUKA code [4].

[1)] The total hadron flux is about an order of magnitude larger since low-energy neutrons dominate the hadron spectrum

To gather information about the changes of hadron spectra two crystals behind each other were considered. A gap of 2 cm was left between the crystals. Support structures or other surrounding material was not considered in the simulations, i.e. the crystals were just floating in the air.

The beam was incident on the front face of the first crystal along its long axis and centered with the crystal.

It is assumed that the average beam intensity is 2×10^{10} p/s.

3.1 Fluxes, stars and dose

The hadron fluxes, stars (hadronic interactions) and dose in the crystal were scored in 1 mm wide bins averaged over the full cross-sectional area. Especially in the front of the first crystal this might slightly underestimate the dose in the center and correspondingly overestimate at the edges. Further back in the crystal scattering and production of secondaries reduce this effect. A plot of these three quantities can be seen in Fig. 1. We can observe a fast increase of all three quantities over the first 5 cm, followed by a slow decrease. The maximum appears so close to the front face because many of the secondaries leave the crystal through the side faces and thus prevent the development of a normal hadronic cascade.

For a pencil beam hitting the center of the crystals (and neglecting any secondaries) we would expect a charged flux of $1/2.6^2$ cm^2=0.148 cm^{-2}. The first plot in Fig. 1 shows about 0.13 cm^{-2}, which is in good agreement because some of the protons in the Gaussian beam miss the crystal while part of this loss is compensated by secondaries. The average charged hadron flux in the first crystal is about 0.2 cm^{-2} per proton. With 2×10^{10} p/s this gives 4×10^9 cm^{-2}s^{-1} and for a 10-hour irradiation an integrated fluence of 1.4×10^{14} cm^{-2}.

The star density per proton reaches to about 0.02 cm^{-3}, which corresponds to about 3 stars per proton in the full crystal. However, this would be higher in a full crystal matrix where the laterally escaping flux is compensated by in-scattering. On the other hand the 24 GeV/c beam is far more energetic than the spectrum in CMS, which probably more than compensates for the out-scattering. **** this might be good to check for a final paper**** The energy threshold for star scoring was set to 20 MeV.

The dose varies between 0.1 nGy/p and 0.25 nGy/p. The average over the first crystal is roughly 0.2 nGy/p. With 2×10^{10} p/s this corresponds to 14.4 kGy/h. For a 10 hour irradiation the integral is in good agreement with the expected 200 kGy in the CMS endcap at η=2.9. Of course – due to compression of 10 years of LHC into 10 hours – this dose rate is four orders of magnitude higher than in the real case and 6 orders of magnitude above the expected barrel dose rate at which most irradiation tests have been performed so far.

3.2 Hadron spectra

The hadron spectra were scored in 2 mm thick slices positioned just in front the the crystal, in its middle and at the back end. Thus for the two crystals there were 6 slices in total. Each slice covered the full cross-sectional area.

The scoring was divided into 4 hadron types: neutrons, protons, pions and all hadrons with strange flavour, i.e. mostly kaons with some contamination by hyperons. Thus this spectral scoring excludes antiprotons and antineutrons. Their contribution, however, is negligible.

The spectral distributions are shown in Figs. 2, 3, 4 and 5.

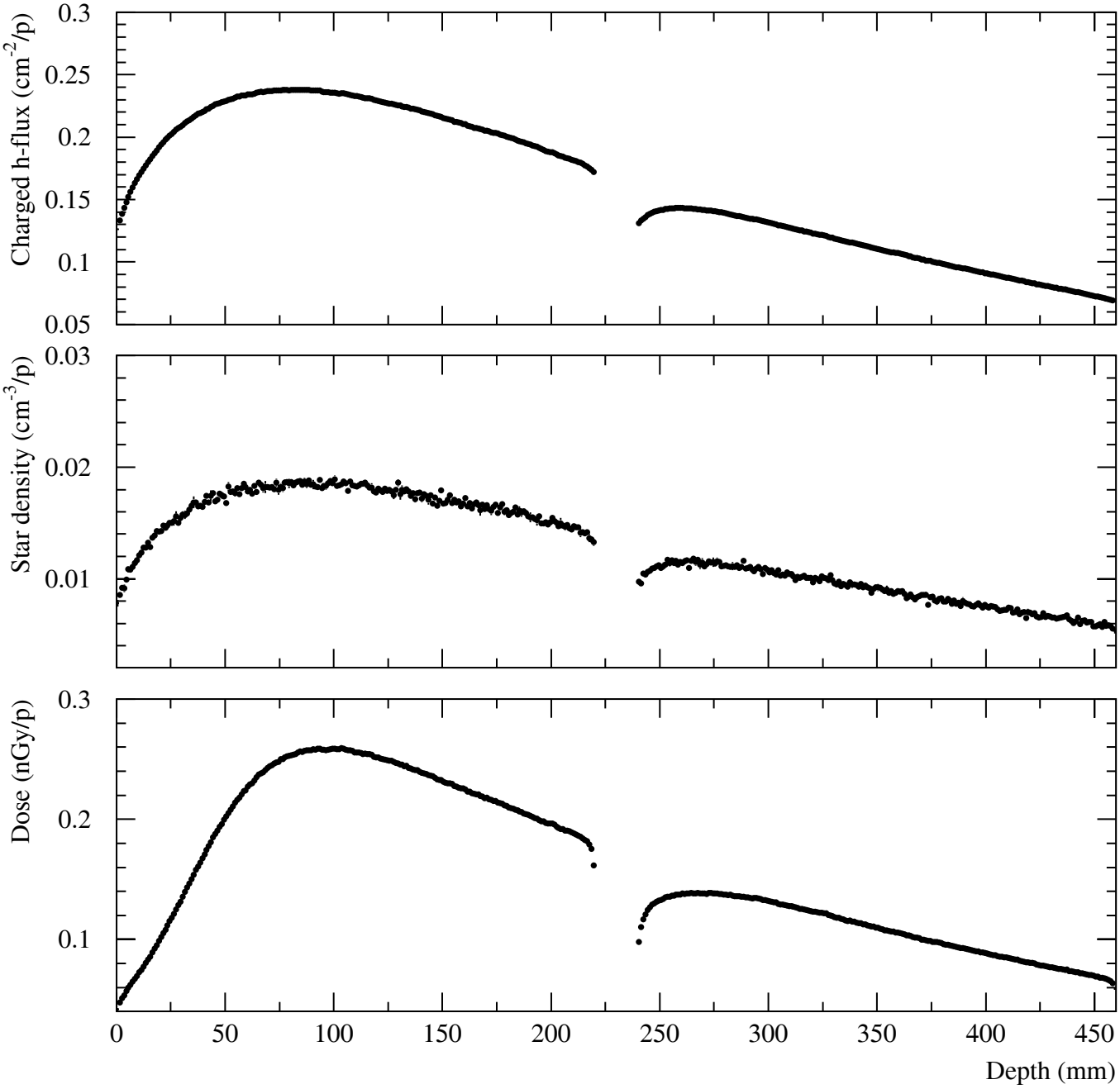

Figure 1: Charged hadron flux, star density and dose as a function of depth in the crystal assembly.

3.3 Induced radioactivity

Due to the hadronic interactions, the crystal will become radioactive. In a previous measurement [1] done at PSI with 355 MeV/c pions a γ-activity of 3×10^6 MeV/s was measured immediately after the irradiation for a 15 g sample of $PbWO_4$. However, the PSI test used a flux of only 2.6×10^7 cm^{-2}s^{-1}. In the PS test the flux would be more than 2 orders of magnitude higher. Since the activity to a first approximation scales with the intensity of the irradiation, we could expect a γ-energy emission rate of

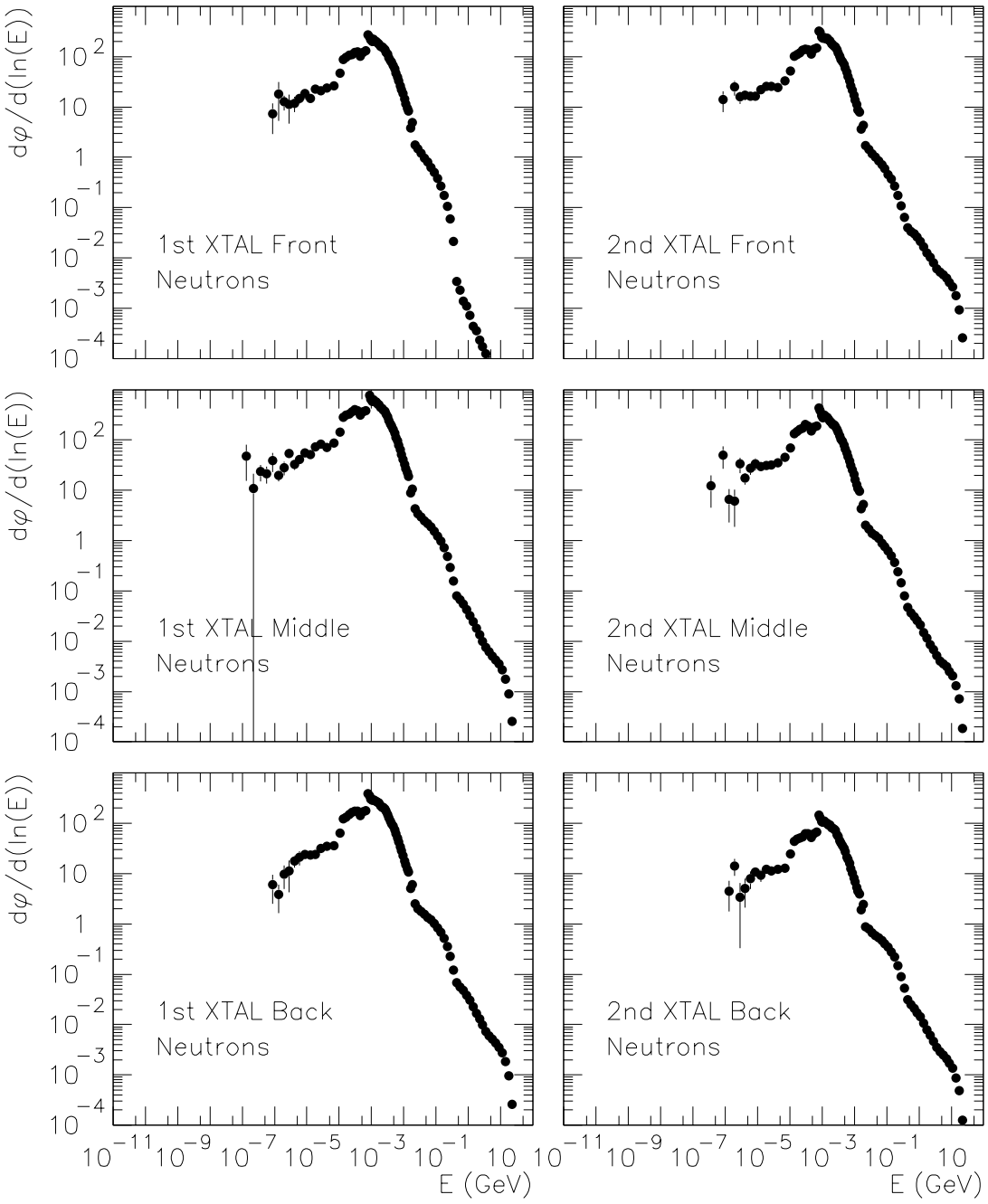

Figure 2: Neutron spectrum in the crystal assembly

roughly 2×10^{10} kev $g^{-1}s^{-1}$ immediately after the PS irradiation. If the whole mass (1230 g) of the crystal would be concentrated in a point source without any self-attenuation, the dose rate at 10 cm distance from the source would be 0.34 Sv/h.

To check this rough rescaling of the previous experimental result a simulation of the induced radioactivity in the crystal was performed. This was done with the same methods which were bench-marked against the PSI activation test.

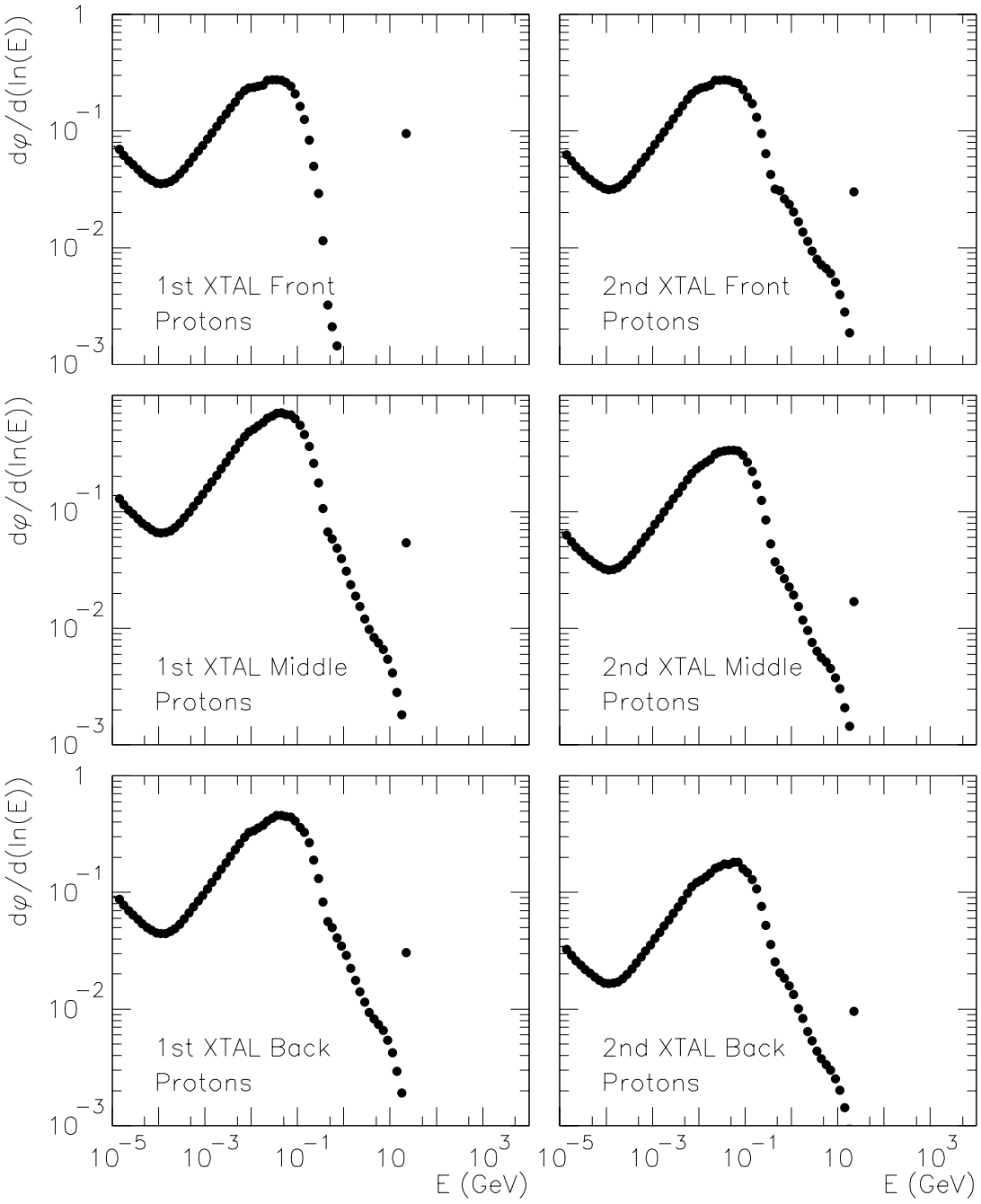

Figure 3: Proton spectrum in the crystal assembly

The residual nuclides in the crystal were scored in the first half of the first crystal[2)].

Since self-attenuation is non-negligible the spatial distribution of the activity is also relevant. In order to take this into account the total residual nuclide yield in the half-crystal was normalized by the total hadron flux in the corresponding region. A 3-dimensional map of the hadron flux with $2\times2\times2\,\mathrm{mm}^3$

[2)] Similar scorings were done for the second half and both halves of the second crystal, but for simplicity only the first scoring was used in the analysis.

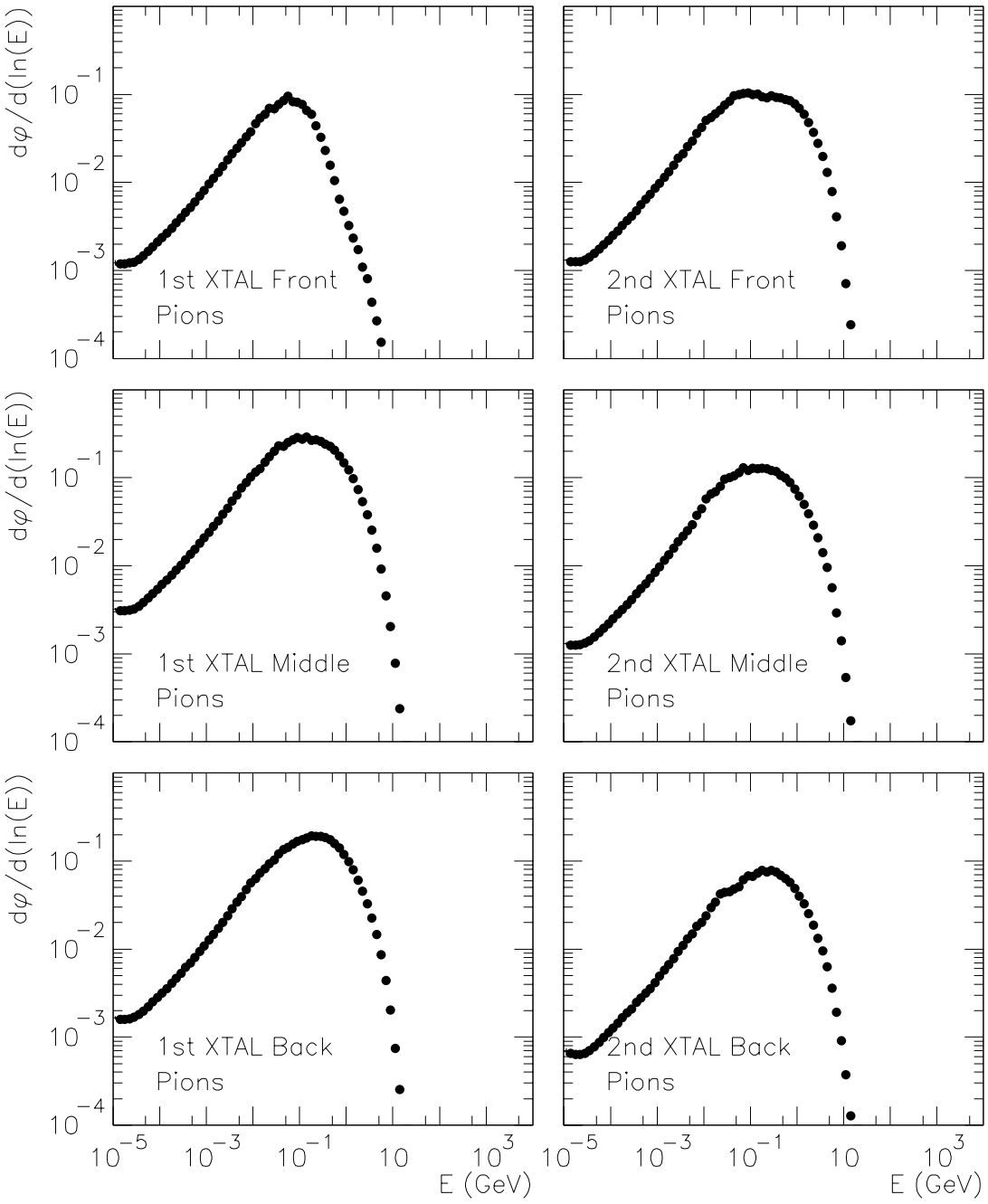

Figure 4: Pion spectrum in the crystal assembly

accuracy was then used to estimate the activity as a function of position in the crystal. To obtain from this the dose at a certain distance a spatial integral over the full crystal was performed. This integral is based on the formula

$$D[Sv/h] = \frac{10^{-8} EA}{7r^2} \exp(-z), \tag{1}$$

where r is the distance from the (point) source in cm, EA is the γ-energy (MeV) emitted per second and z is the number of attenuation lengths between the source and the point of observation, i.e. $z = r/\lambda$,

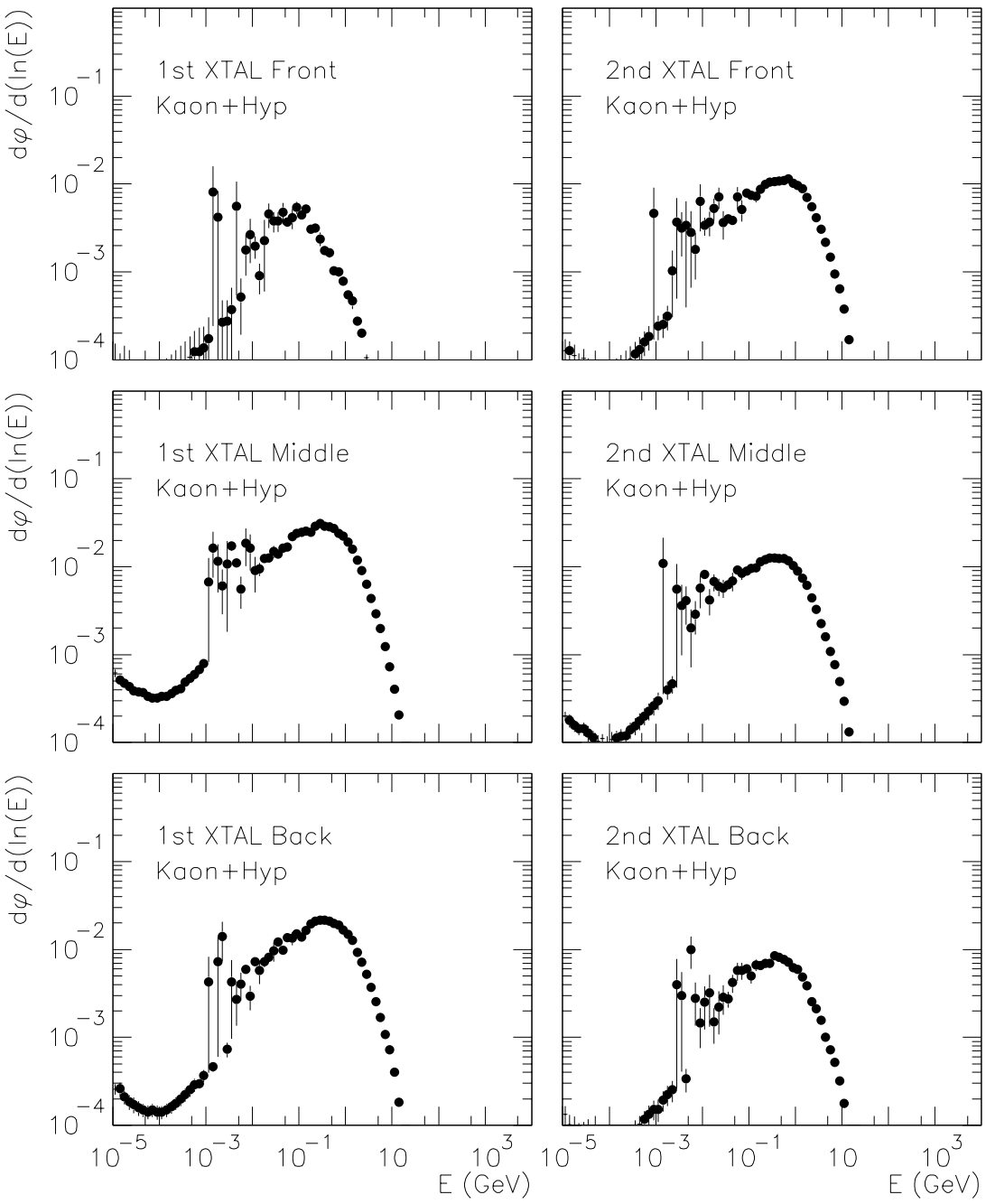

Figure 5: Kaon (+hyperon) spectrum in the crystal assembly

where λ is the attenuation length. This narrow beam attenuation slightly underestimates the dose because it does not account for build-up. This can be corrected by multiplying Eq. 1 with simple parametrisation of the form

$$1 + a\exp(bz), \tag{2}$$

where a and b are parameters which depend in the material and the energy of the γ-ray. It has been shown that over reasonable depths the attenuation characteristics of a typical induced activity spectrum follow that of monoenergetic γ-rays of about 1 MeV of energy. At this energy and for $PbWO_4$ the parameters

take the values $\lambda = 1.95$ cm, $a = 0.465$ and $b = 0.0284$.

In the vicinity of the crystal the dose maximum is reached in the center of one of its long faces. This position is used in Fig. 6, which shows the dose rate due to induced radioactivity as a function of time for various distances to the center of the crystal. The activity of any individual radionuclide – neglecting the effects of decay chains – can be described by

$$A \propto \frac{P}{\lambda}[1 - e^{-\lambda t_i}]e^{-\lambda t_c}, \tag{3}$$

where P is the production rate, λ the decay constant and t_i and t_c the irradiation and cooling times. Setting $t_c = 0$, we can see that saturation is reached when $t_i \gg 1/\lambda$. Practical saturation (95% of asymptotic value) are reached after 3 decay constants, i.e. 4.3 half-lives. This means that after 10 h of irradiation all nuclides with half-lives of 2 h or less will be in saturation. Such short-lived nuclides dominate the activity during irradiation so that Fig. 6 indicates almost full saturation already after 10 hours of irradiation. However, because this activity is mostly due to the short-lived nuclides the decay of dose rate is very fast.

This is fortunate because immediately after irradiation the crystal shows contact dose rates in excess of 1 Sv/h. Even at 10 cm distance the dose immediately after the irradiation is about 500 mSv/h. This is in sufficiently good agreement with the rough estimate based on the previous pion activation test.

More important than the dose rate immediately after the irradiation is the dose rate after a reasonable cooling time. It can be seen that 14 h after the end of irradiation (1 day in Fig 6) the contact dose is still at a dangerous 200 mSv/h level, but the dose at 50 cm distance has dropped to 1 mSv/h. This is still problematic for longer manipulation. It might be more reasonable to foresee measurements of the crystal after a cooling of about 10 days. By that time the dose at 50 cm distance has dropped to about 50 μSv/h and the contact dose to few mSv/h. After 1 month of cooling the contact dose is at the 1 mSv/h level.

For the planed test a waiting for cooldown should not be too serious because the main objective is to verify if hadrons produce stable accumulative damage. In the real LHC conditions the full fluence will be accumulated during 10 years, thus any annealing with time constants of months or even a year, will have taken place. Therefore this test actually *should* aim at an observation of possible damage after an extended cooling period.

The possibility of specific hadron damage with short time constants should be studied separately at proper LHC fluxes and correspondingly much lower integrated fluence. Actually exactly this type of test has been performed in 1998 and no anomalies were observed [2].

References

[1] P.A.Aarnio, T.T.Hakulinen and M.Huhtinen, J. Radioanl. Nucl. Chem. 248 (2001) 385.

[2] E.Auffray *et al*, CERN CMS NOTE 98/069 (1998).

[3] P. A. Aarnio, CERN CMS NOTE-1998/086 (1998).

[4] P. A. Aarnio *et al*, CERN TIS-RP/168 (1986) and CERN TIS-RP/190 (1987).
A. Fassò *et al*, Proc IV Int. Conf. on Calorimetry in High Energy Physics, La Biodola, Sept 20-25, 1993, Ed. A. Menzione and A. Scribano, World Scientific, p. 493 (1993).
P. Aarnio and M. Huhtinen, Proc MC93, Int. Conf. on Monte Carlo Simulation in High Energy and Nuclear Physics, p 1, ed. P. Dragowitsch, S. Linn and M. Burbank, World Scientific (1994).

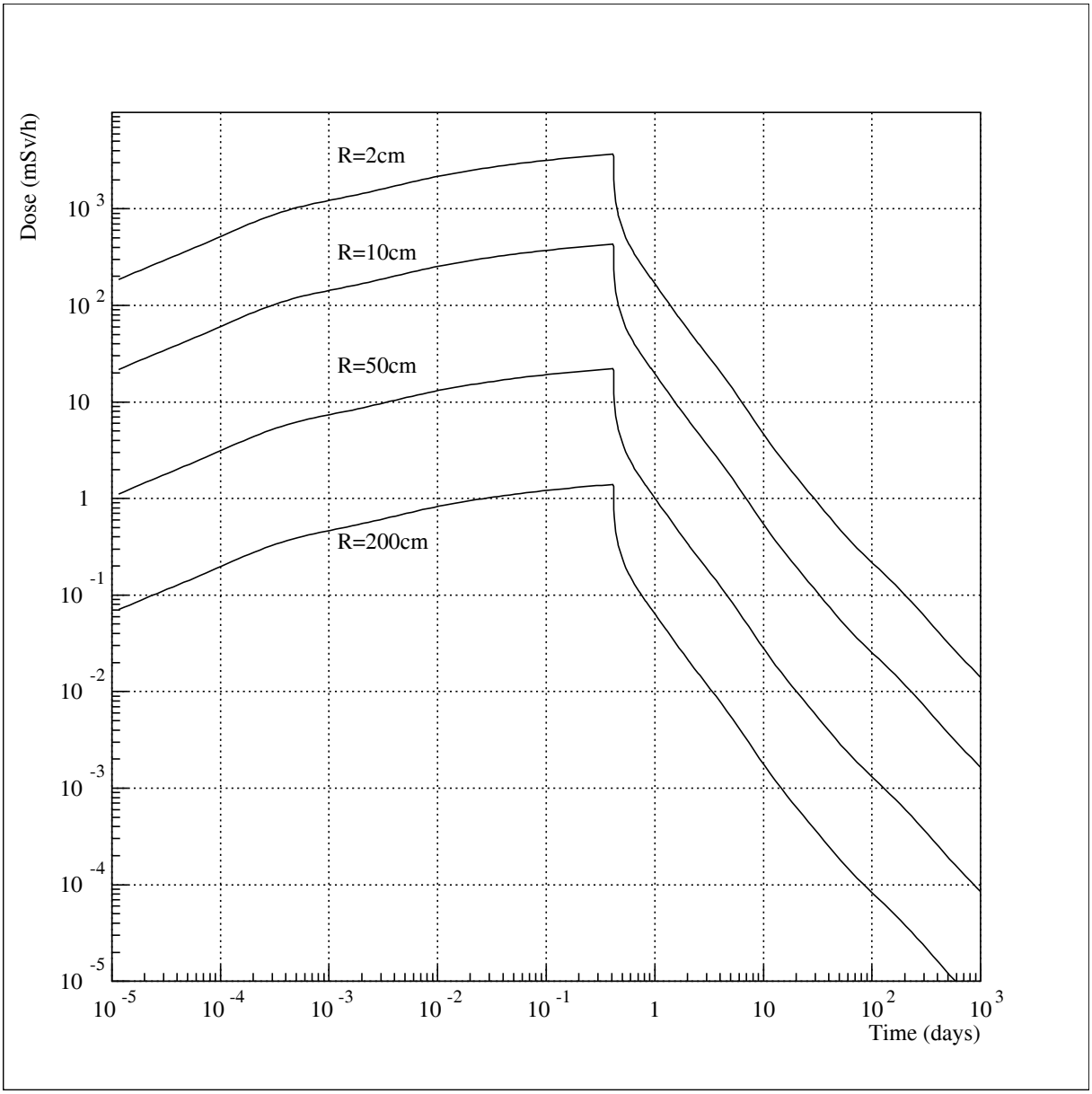

Figure 6: Dose rate due to induced radioactivity in the crystal. The plots correspond to the center along the long face of the crystal and the indicated distance from the crystal axis.

A. Fassò *at al*, Specialists' Meeting on Shielding Aspects of Accelerators, Targets and Irradiation Facilities. Arlington, Texas, April 28-29, 1994. NEA/OECD doc. p. 287 (1995).

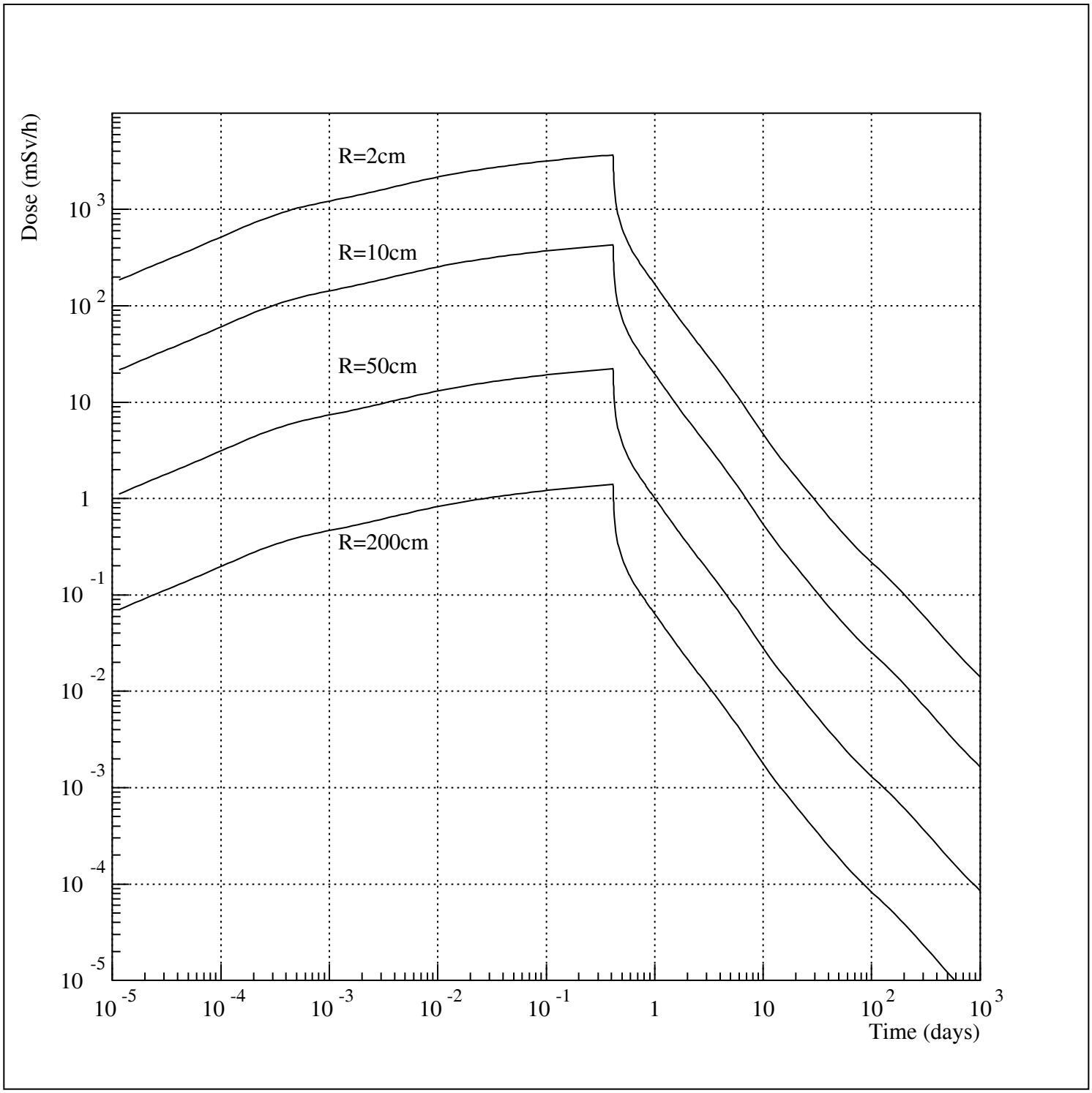
Dose (mSv/h)
R=2cm
R=10cm
R=50cm
R=200cm
10 3
10 2
10
1
10 -1
10 -2
10 -3
10 -4
10 -5
10 -5
10 -4
10 -3
10 -2
10 -1
1
10
10 2
10 3
Time (days)

ETH Zürich

Monitored irradiations of EE 2461at PSI-Eichlabor

P. Lecomte and F. Nessi, ETH-Zürich

CMS

- 40 TBq 60Co source = a movable table in a 12 m deep room (dose rates adjustable through distance from 4 Gy/h down)

- The relative light yield loss due to irradiation is measured, using a weak calibration source (typically 60Co) to excite scintillation. As a light detector,a XP2262B photomultiplier with a CERN base is used, installed in a 3 cm thick Lead cylinder.

- The crystal is irradiated from the side. For such a long crystals, the photocathode is recessed by 8 cm, and the rest of the crystal stick out of the shield and are irradiated.

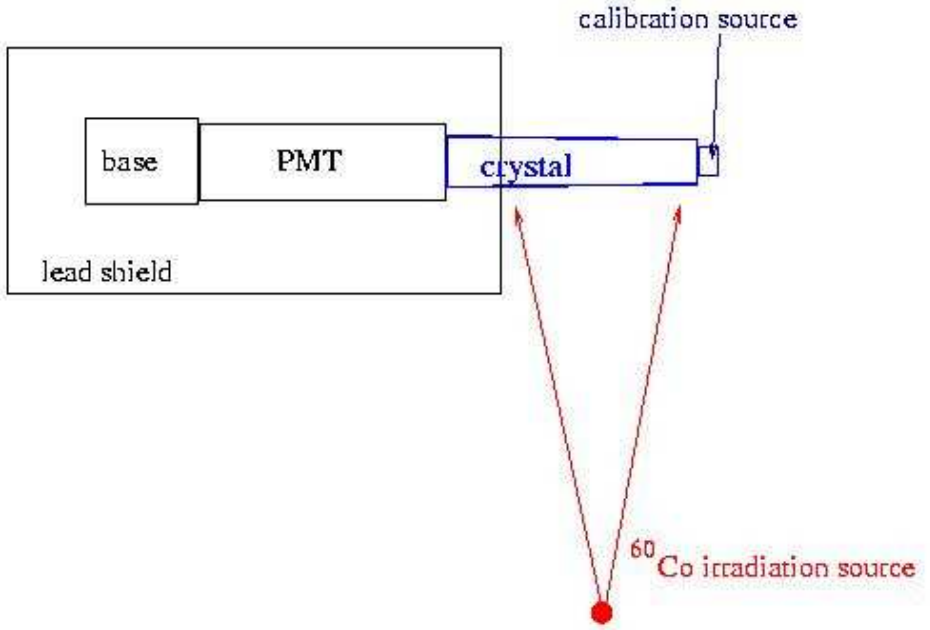

H.F.Chen, K. Deiters, H.Hofer, P.Lecomte, F.Nessi-Tedaldi, NIM 414 (1998) 149-155

ETH Zürich

Setup at the PSI Eichlabor

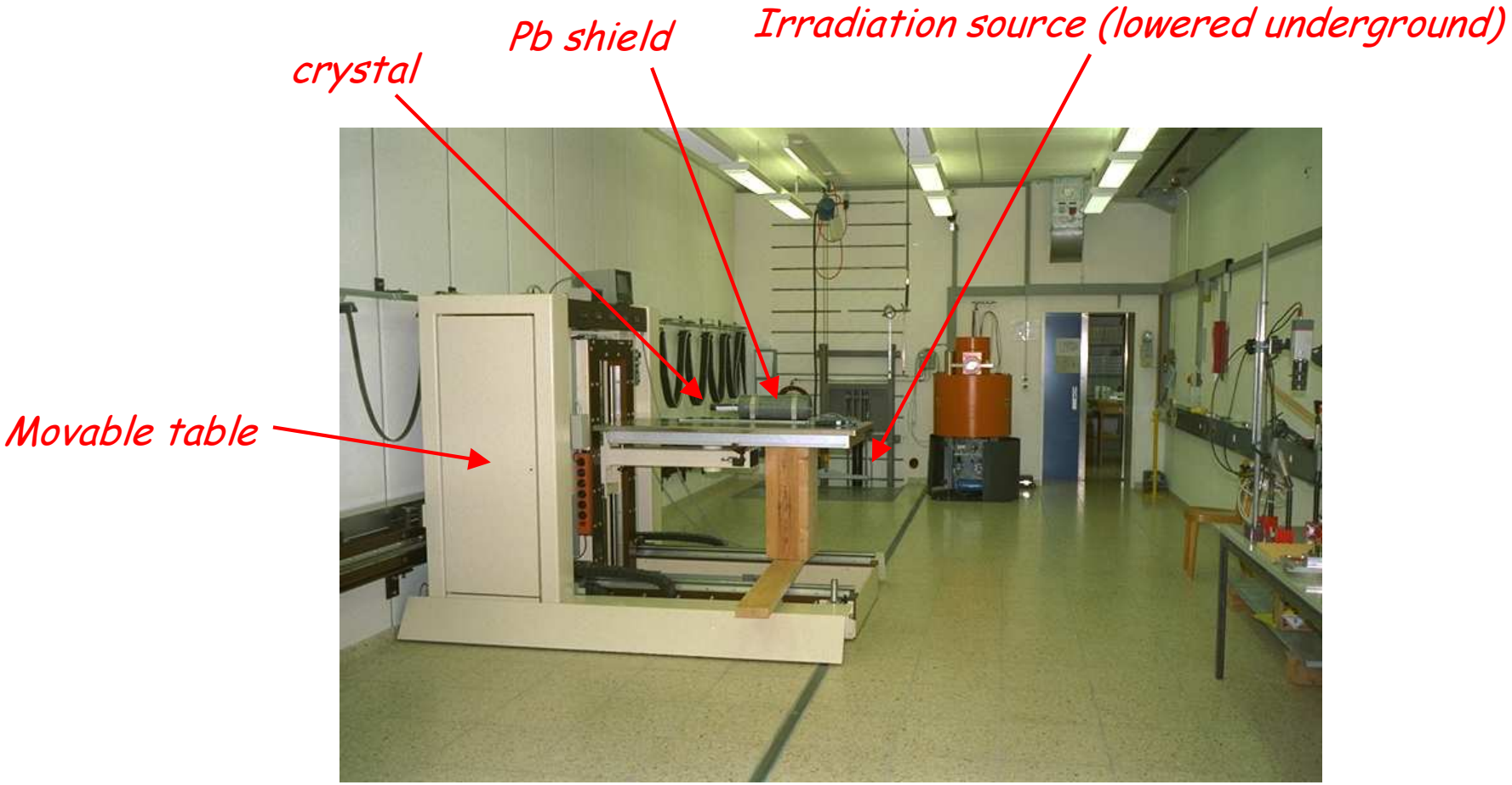

ETH Zürich

Progress on uniformity of recent EE crystals from BTCP

CMS

- Typical cycle of measurements:
- Crystals is mounted in place, a weak source exciting scintillation.
- It is left thermalising for ~ 12 h, while scintillation spectra are taken every 10 min.
- PM HV is turned off. An irradiation lasting 30 min (resp. 60 min) is performed. When the irradiation stops, PM HV is turned on within a few seconds, and 3 spectra are taken.
- The cycle is repeated until saturation of damage is reached (typically 12 h)
- Crystal is left in place, for monitored recovery (spectra are taken every 10 min)

For this crystal we performed:

→ Thermal stabilisation

→ 1.125 Gy at 0.15 Gy.h + overnight recovery

→ 4 Gy at 0.4 Gy/h + overnight recovery

→ 7.5 Gy at 1 Gy/h + overnight recovery

→ 30 Gy at 4 Gy/h + overnight recovery

ETH Zürich

Irradiation results for EE 2461 (part I of IV)

Bogo EE2461 thermalization before 1st irradiation 22/23-AUG-2001

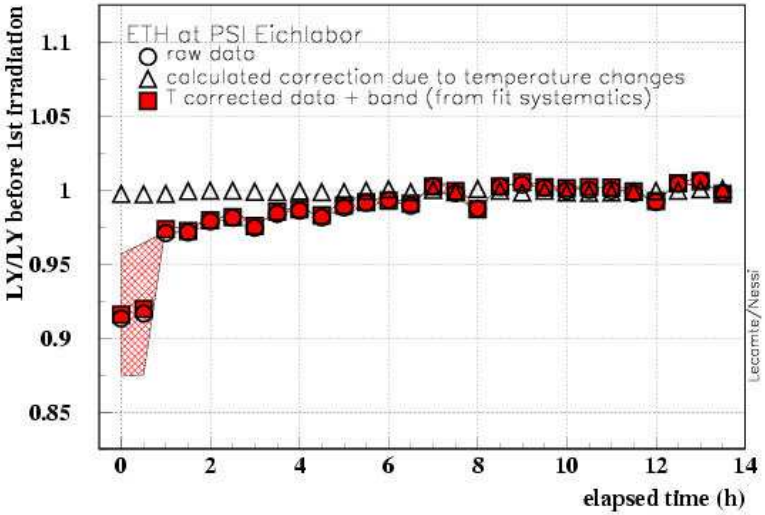

Bogo EE2461 during 1st 60Co irradiation 23-AUG-2001

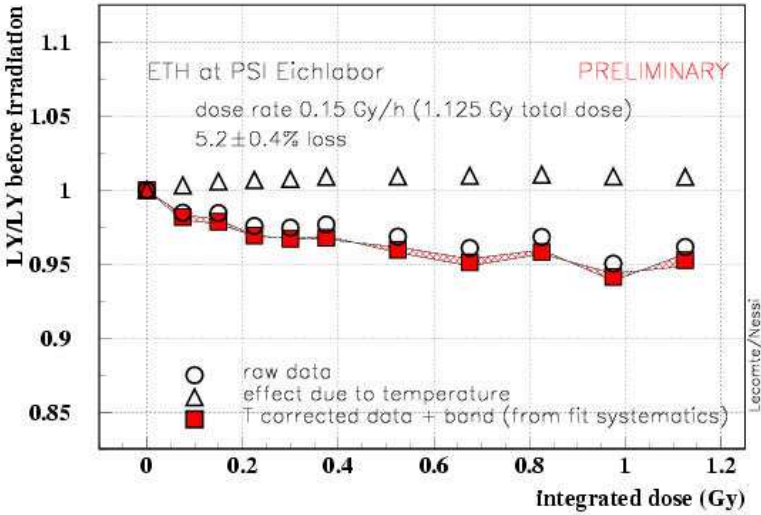

(5.2 ± 0.4)% loss at 0.15 Gy/h

followed by full recovery, with

τ = 7.4 ± 2.2 h

Recovery of Bogo ee2461 after 60Co irradiation 23/24-AUG-2001

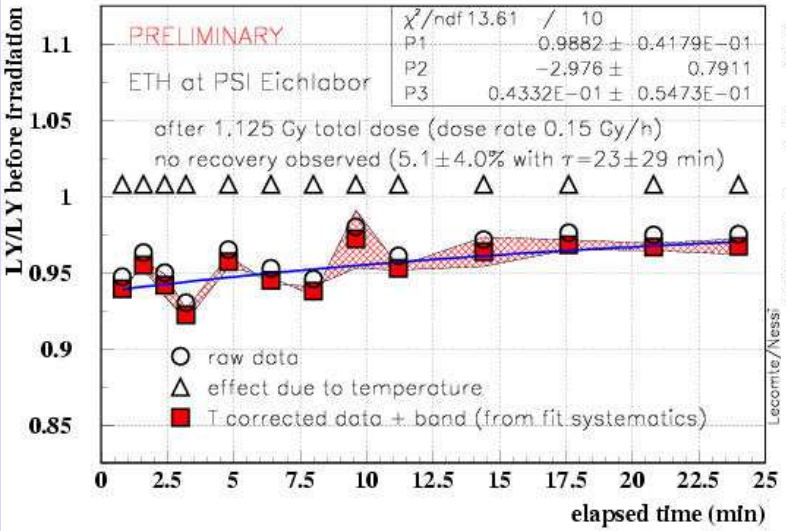

Bogo EE2461 recovery before 2nd irradiation 23/24-AUG-2001

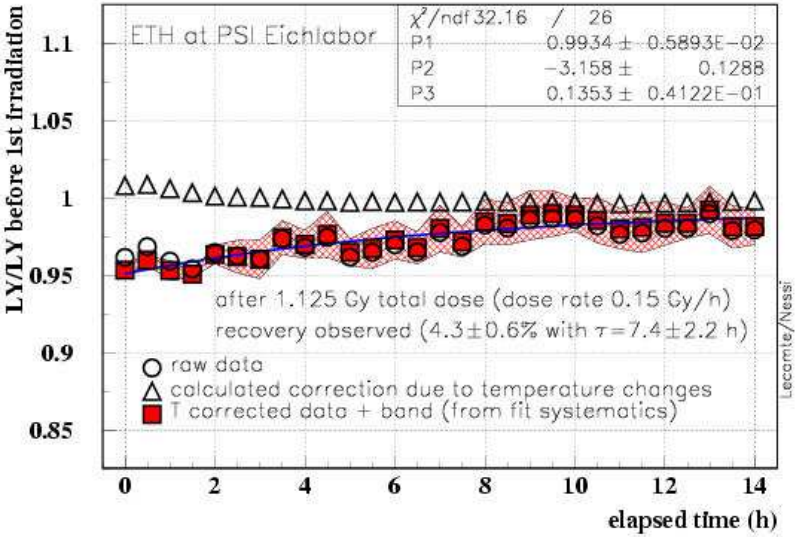

PRELIMINARY

ETH Zürich

Irradiation results for EE 2461 (part II of IV)

CMS

Bogo EE2461 during 2nd 60Co irradiation 24-AUG-2001

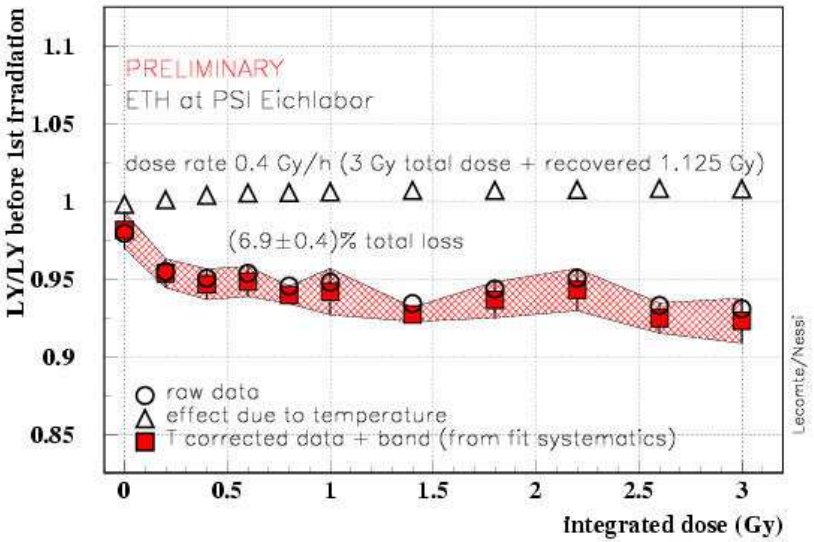

Recovery of Bogo ee2461 after 2nd 60Co irradiation 24-AUG-2001

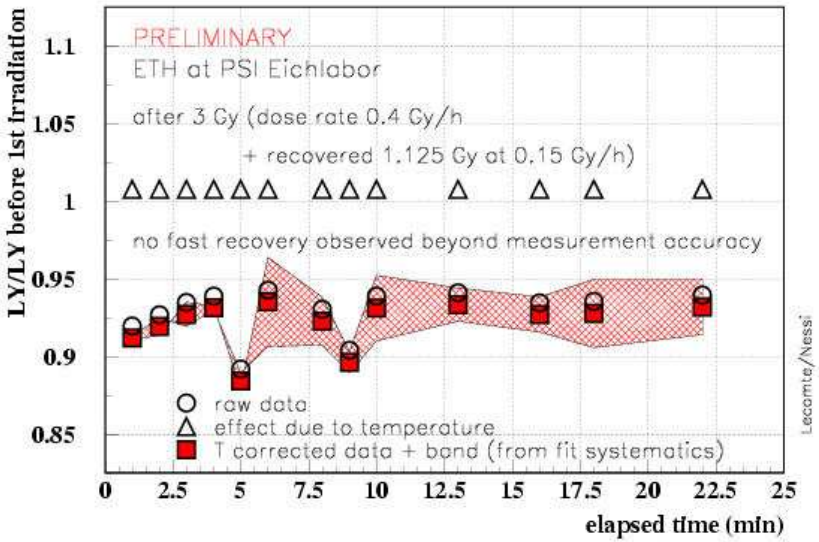

Bogo EE2461 recovery before 3rd irradiation 24/25-AUG-2001

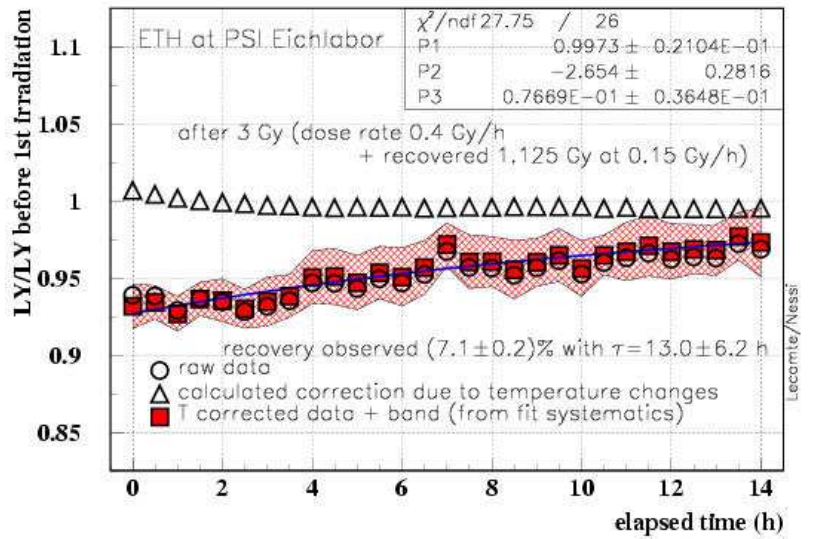

(6.9 ± 0.4)% loss at 0.4 Gy/h

almost full recovery overnight, with

$\tau = 13.0 \pm 6.2$ h

PRELIMINARY

Irradiation results for EE 2461 (part III of IV)

ETH Zürich

Bogo EE2461 during 3rd 60Co irradiation 25-AUG-2001

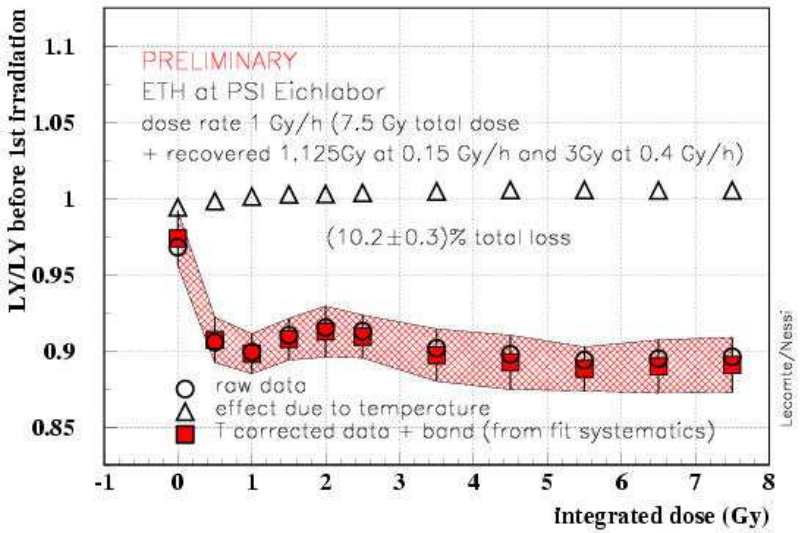

Recovery of Bogo ee2461 after 3rd 60Co irradiation 25-AUG-2001

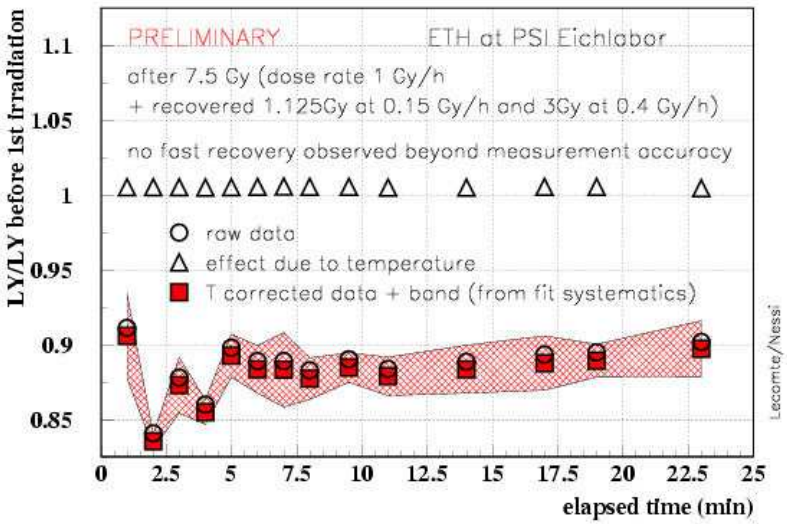

Bogo EE2461 recovery before 4th irradiation 25/26-AUG-2001

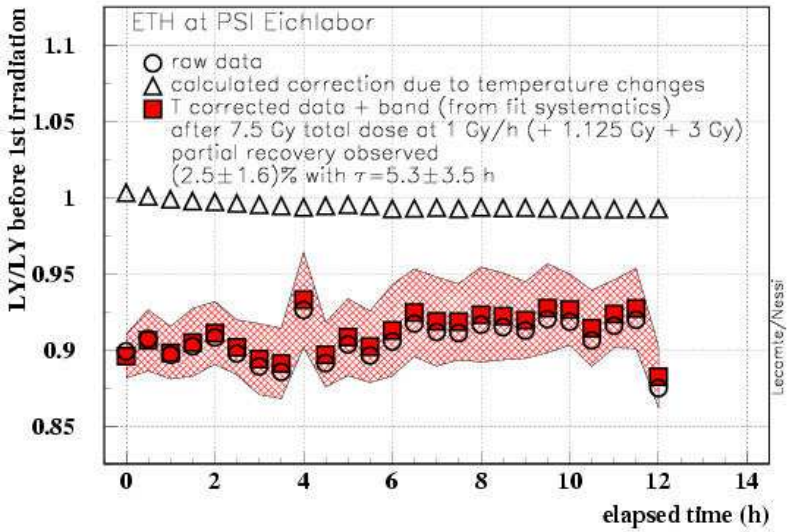

(10.2 ± 0.3)% loss at 1 Gy/h

followed by partial recovery overnight, with

τ = 5.3 ± 3.5 h

PRELIMINARY

ETH Zürich

Irradiation results for EE 2461 (part IV of IV)

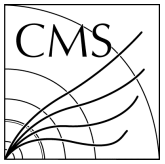

Bogo EE2461 during 4th 60Co irradiation 26-AUG-2001

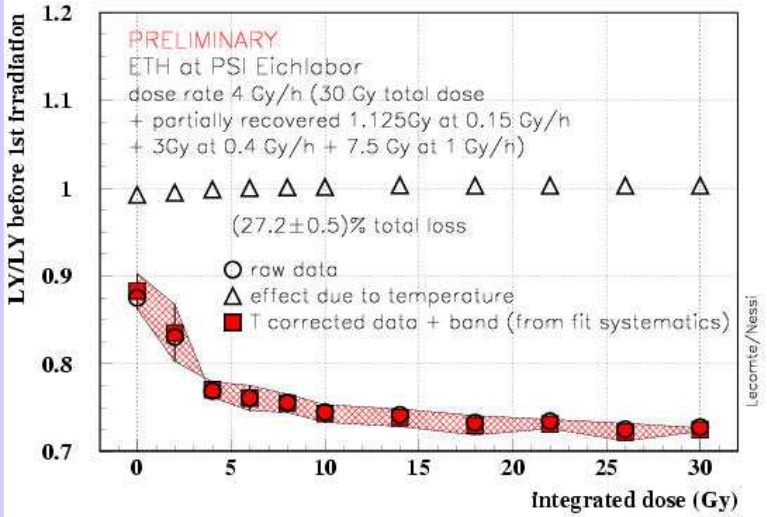

Recovery of Bogo ee2461 after 4th 60Co irradiation 26-AUG-2001

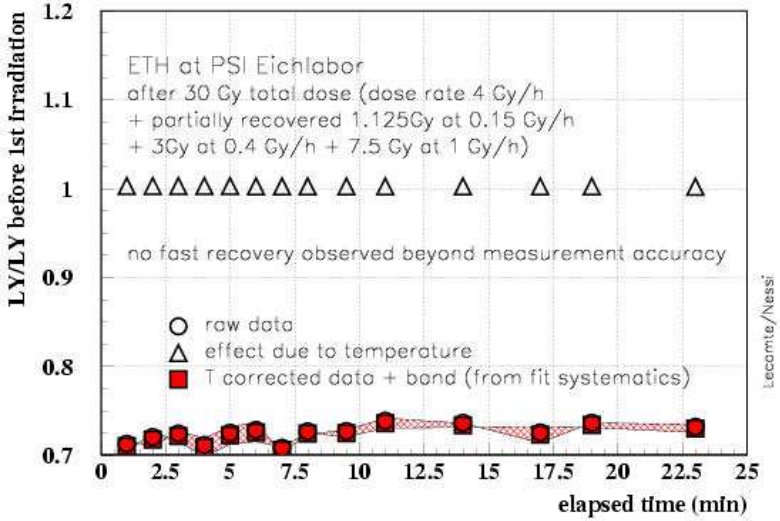

Bogo EE2461 recovery after 4th irradiation 26/27-AUG-2001

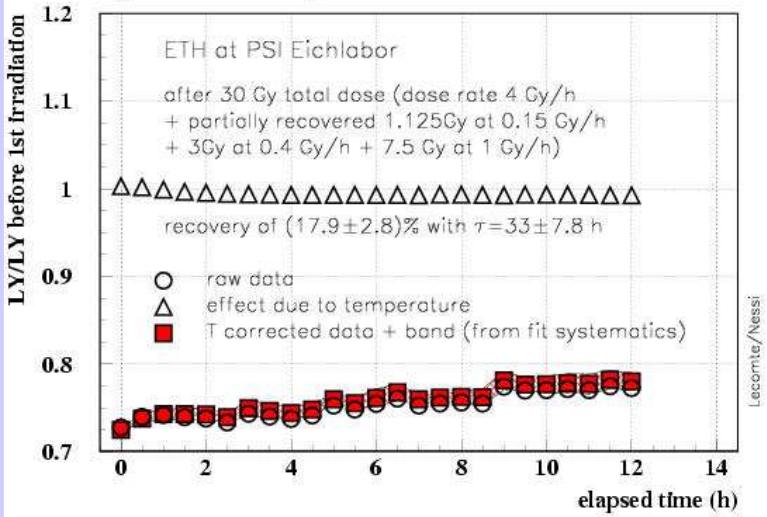

(27.2 ± 0.5)% total loss at 4 Gy/h

followed by partial recovery overnight, with

τ = 33 ± 7.8 h

PRELIMINARY

ETH Zürich

Progress on uniformity of recent EE crystals from BTCP

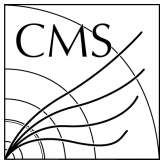

PRELIMINARY

BarCode	LT360	LT420	LT620	slope	Dispersion TTO	LY	Fnuf	Rnuf	gradTT
30399000000461	40.97	71.47	75.84	3.361	0.661	12.59	0.175	0.011	-0.004

Dose rate (Gy/h)	Integrated dose (Gy) *	LY loss** (%)	Recovery amplitude (%)	Recovery time constant#
0.15	1.125	5.2 ± 0.4	full	7.4 ± 2.2 h
0.4	3	6.9 ± 0.4	full	13.0 ± 6.2 h
1	7.5	10.2 ± 0.3	partial	5.3 ± 3.5 h
4	30	27.2 ± 0.5	partial	33 ± 7.8 h

* At the given dose rate (effect from previous irradiations partially recovered overnight

** Total loss with respect to LY before first irradiation

Fit using just one exponential

fast recovery measurents not significant, should be checked on other setups (CERN/TIS?)

CMS NOTE 1998/044

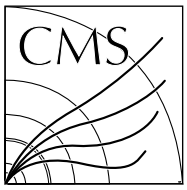

The Compact Muon Solenoid Experiment

CMS Note

Mailing address: CMS CERN, CH-1211 GENEVA 23, Switzerland

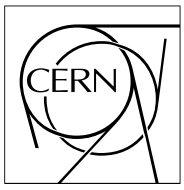

July 29, 1998

Production of long-lived radionuclides in CMS

Mika Huhtinen

CERN, CH-1211 Geneva, Switzerland

Pertti A. Aarnio

Helsinki University of Technology, FIN-02015 HUT, Finland

Abstract

We discuss the production of radionuclides which are of significance when assessing the amount of radioactive material to be deposited or recycled after decommissioning of CMS. Our estimate is based on a detailed accounting for each individual radionuclide and accurate follow-up of the time dependence of the activity. Compared to a previous study using crude parametrizations the new results indicate significantly lower amounts of radioactive material. According to the new estimate the amount of active (>1 Bq/g) material from CMS, 30 years after LHC shutdown, will be 150 tons. Only the collimators, none of the CMS proper, will fall into the >100 Bq/g category after 30 years of cooling.

Category			
0	1	2	3
<1 Bq/g	1–10 Bq/g	10-100 Bq/g	>100 Bq/g
$<1\,\gamma$-MeV/g/s	1–10 γ-MeV/g/s	10-100 γ-MeV/g/s	$>100\,\gamma$-MeV/g/s

Table 1: Activity categories according to the specific activity or the γ-energy emission rate. These two are not equivalent and the latter has been introduced only to illustrate better the radiological implications.

1 Introduction

All materials at a hadron collider will inevitably get activated by hadronic interactions. Compared to nuclear reactors or other facilities where activation can occur the accelerator environment is unique in the sense that even from a single target isotope a multitude of radionuclides can be produced. This is due to spallation reactions where a random number of nucleons are removed from the nucleus. In cases where the corresponding threshold is exceeded, high-energy fission or multifragmentation can result in several radioisotopes from one interaction. On the other hand not all interactions give a radioactive isotope, in some cases the residual can be directly a stable nuclide. Also most of the formed radioisotopes have short half lifes and disappear rather quickly. Some of them, however, remain for extended periods in the structures, which thus have to be considered radioactive material. Depending on the specific activity different disposal schemes have to be planed for the activated components. In order to foresee sufficient resources for the decommissioning it is important to have an estimate of the amount, the specific activity and the effective activity decay time of the detector components.

A first estimate of the amount of radioactive material produced in CMS [1] was based on some crude parametrizations, namely the ω-factors [2, 3] and the Overton-Sullivan formula [4]. Although these methods have been well established during the past 30 years, two reservations were made in [1], calling for a more detailed analysis. The reservations were:

1. The Overton-Sullivan formula has been fitted to iron type material up to few years of irradiation and cooling time. It gets pushed over its limits when applied to the LHC case. Thus the error made for the longest cooling times is unpredictable.
2. The ω-factors describe only average dose rate, which is related to the γ-emission rate. In an average way this can be traced back to activity of γ-emitters, but the result does not make any statement about the total activity.

In addition to these reservations it was remarked that total activity, or even total γ-activity, is not a sufficient measure to qualify of quantify the amount of radioactive materials, since individual radioisotopes have very different radiological implications and correspondingly very different exemption limits.

This new study addresses the question in a much more detailed fashion by using explicit radionuclide inventories, although still maintaining a relationship to the star densities, which are the underlying ingredients of ω-factors.

The materials will be divided into four categories, shown in Table 1. It is to be emphasized that the division by γ-energy emission rate does not correspond to the CERN internal classification (by Bq/g), but is added to illustrate some important points of radiological danger.

The major obstacle, when trying to estimate radionuclide production rates at accelerators, is that sufficiently complete cross section data are not available. Although some data can be found for given target material, projectile and energy combinations, we are still far from having a complete cross section library to be used in simulation codes.

The use of available data is tedious hand-work, since inconsistencies have to be checked one by one and often interpolations or extrapolations are required to cover gaps in the data. Therefore this procedure is feasible only for some selected target materials, where sufficient data are available. In practice the only material for which this is the case is aluminium. For iron, which represents most of the mass of CMS, a fairly good coverage of experimental data can be found for protons [5], but the extrapolation of these data to neutrons and pions should be considered an educated guess at its best. For the analysis to be presented in appendix B of this paper such an extrapolation has been done simply by weighting the partial cross sections for protons with the ratio of pion/proton (neutron/proton) total cross sections at the corresponding energy.

For materials heavier than iron an approach based on experimental cross sections is essentially excluded.

We base our analysis for all materials on the residual nuclide yields from the FLUKA [6] simulation code. It must be emphasized that these yields are known to be quite inaccurate for some individual nuclei, especially if the projectile is mono-energetic. If, however, the irradiation consists of several particle types with broad energy spectra the average results seem to agree rather well with similarly averaged cross section data.

2 Simulation Methods

2.1 Assumed LHC luminosity profile

When calculating the induced radioactivity in materials it is of utmost importance to have a fairly realistic assumption of the luminosity profile. We assume that the peak luminosity increases per year from 10% to 33%, to 67% and to 100% in the fourth year. Each year there are three 60 day operating periods separated by 10 days and one long annual shutdown. The average luminosity during one day of operation is half the nominal one. The heavy-ion operation takes place at very low luminosity and is therefore negligible.

2.2 The classical approach

Traditionally dose rate due to induced activity at hadron accelerators has been predicted with some rather crude but empirically verified parametrizations. These are the ω-factors, which describe the induced activity dose rate and the Overton-Sullivan formula, which describes the average decay. The ω-factors are strongly material dependent, but they also have some dependence on the radiation field. In particular they become very unreliable if low-energy neutrons play a significant role in the activation (see appendix B).

The ω-factor postulates that activation is proportional to the rate of inelastic hadronic interactions (stars) above a certain threshold energy, which traditionally has been set to 50 MeV. The ω-factor describes the dose in contact with a semi-infinite slab of material with uniform star density which means that they correspond essentially the γ-dose, although this is not explicitly stated in the definition. In addition the ω-factors are always defined for fixed irradiation and cooling times. The traditional choice is t_i = 30 days and t_c = 1 day.

The extrapolation to other times can be obtained with the Overton-Sullivan formula [4], which is based

on a statistical analysis of the distribution of half-lifes of radionuclides below the iron mass. It predicts that the activity follows a dependence

$$D \sim \ln \frac{t_i + t_c}{t_c}, \tag{1}$$

where t_i is the irradiation time and t_c is the cooling time.

One aspect to note is that the Overton-Sullivan formula is not exactly applicable to a complicated irradiation profile, since the parametrization is valid only for one single constant irradiation.

2.3 Definitions and notations

Since the ω-factors are defined for semi-infinite bodies and uniform star densities they are often difficult to apply to real sitations encountered at accelerators. By assuming a fixed photon energy per decay, the ω-factors can be related to virtual activity per star. In our previous work [1] we have done this by defining one 'Bq' to correspond to the emission of one 800 keV photon. Throughout this report the notation 'Bq' stands for such an emission of one 800 keV photon per second. See appendix B for a detailed discussion between 'Bq' and the ω-factor.

The notation Bq stands for true activity with no reference to energy emission or emitted particle type.

We use the notation γ-MeV/s to indicate the rate of emitted energy in form of photons. Thus, this definition is equivalent to 1.25$\times$'Bq'. Although there is no fixed correlation the γ-MeV/s values will often be numerically rather close to the activities (Bq), because the average γ-energy per decay is a few hundred keV.

It is clear that all of the above, if expressed as a function of star production rates, should be written as Bq/(stars s^{-1}), or if specific activity is considered as Bq cm^{-3}/(stars s^{-1} cm^{-3}). In order to simplify the notation these will be abbreviated to Bq/star, the context will imply the proper units. In analogy with this 'star density production rate' will be abbreviated to 'star density' in the text. In this context it should be reminded that the level of induced activity for a given nuclide is not a function of the amount of radionuclides produced but of both, the production rate and the duration of the irradiation. For sufficiently long irradiation times the activity reaches saturation and is equal to the production rate.

2.4 High-energy activation

A practical problem in estimating radionuclide production in a complicated system like CMS, which is exposed to a very inhomogeneous radiation field, is that the production rates will be strongly position dependent. Assuming that the CMS area is divided into rz-bins of 10$\times$10 cm^2, which is a maximum still able to reasonably reproduce the variation of geometry and radiation field gradients, the number of bins exceeds 30000. Still this assumes symmetry with respect to the z=0 plane as well as full ϕ-symmetry, In each bin one would have to score all residual nuclides. The number of these can exceed 1000 in the case of lead and is typically several hundred for iron. While some 10 MB of data would not be unbearable, all bins would suffer from poor statistics so that some averaging would be unavoidable.

A more elegant, although slightly approximate, way is to assume that the radionuclide production is proportional to the number of inelastic interactions above a certain energy threshold. This assumption is identical to the definition of ω-factors. We, however, do not restrict ourselves to the average treatment, characteristic for the ω-factors, but derive explicitly the production rates for individual nuclei. Thus, instead of the contact dose, we will parametrize the yield of each individual radionuclide as a function of the star density.

This is achieved by scoring residual nuclei in FLUKA by material, and not by region or spatial bin. In CMS, 9 materials represent most of the detector mass, so we arrive at only 9 radionuclide inventories. Since these are scored in all the volume filled with the corresponding material, the statistics is as good as it can get in a given simulation. Simultaneously the number of stars is scored in the same materials. This allows to calculate the production rates per star for each individual isotope. The spatial variation is then obtained by scoring stars, which is a nice scalar quantity, in a spatial binning.

The approximation implicitly included in this approach is, much like for the ω-factors, that the production rate of any individual radionuclide produced in an inelastic interaction is independent of the spectrum in the range over which the spectrum varies as a function of position. It should be emphasized that this is a much better approximation than to scale the production rates to particle flux, because the stars take the energy dependence of the total inelastic cross section into account. This issue is discussed in detail in appendix B, where it is shown that some spectral dependence remains as an uncertainty in the results[1)].

2.5 Low energy neutron activation

Low energy neutrons, in this context, are defined as those below 20 MeV of kinetic energy. This is a practical limit, since only up to 20 MeV almost complete cross-section data are available so that fairly accurate simulation of neutron transport and interactions is possible. All hadrons above 20 MeV are treated by the high-energy modules of the FLUKA code.

If only long-lived (half-life longer than some 100 days) radionuclides are considered, only few low-energy neutron activation channels need to be considered for the bulk materials we foresee in CMS.

Table 2 shows the neutron reactions which have been considered. For the (n,p), (n,d) and (n,α) reactions the energy dependence of cross sections is taken into account. The spatial fast neutron flux scoring in FLUKA, however, was done with a 1 MeV threshold, which agrees rather well with most reaction thresholds. Correspondingly the production probabilities have been normalized with the neutron flux above 1 MeV, no matter what the actual energy dependence of a given channel. The (n,γ) reactions are assumed to take place only in the thermal group of FLUKA leading to a straightforward flux normalization.

It should be noted that the reactions listed in Table 2 correspond to the ideal case of pure bulk materials. In particular stainless steel, which typically contains nickel and chromium is not considered explicitly. The amount of stainless steel in CMS, however, is relatively small. All steel is assumed to contain 1% of nickel, which should give a reasonable overall approximation. These results can be refined once the final composition of various steel parts is decided.

The amount of impurities, which might allow other reactions, is not known for the moment. The effects of even relatively small impurities can be significant for neutron activation, where cross sections can vary by orders of magnitude between neighbouring isotopes. The classical example is cobalt contamination of steel, which can be used to provide one example of the possible effects: the thermal activation cross section is $\sigma = 3.7 \times 10^4$ mb. If we denote the thermal neutron flux as ϕ and the weight fraction of cobalt as w, we get the saturation activity of ^{60}Co as:

$$A = \frac{1}{4}\phi\frac{N_A \sigma w}{A} = 0.0925 \left[\frac{\mathrm{cm}^2}{\mathrm{g}}\right] \phi w, \tag{2}$$

where the factor of 1/4 scales from the peak luminosity to a long-term average. With a typical value of

[1)] In appendix B a different star definition with 20 MeV threshold is proposed. All simulations for this study, however, were done before this observation and the relatively small difference did not seem to justify a repetition of the time-consuming simulations. Thus, despite the findings detailed in appendix B, stars in this work are still defined with a 50 MeV threshold.

Material	Thermal n	Fast n
Steel	^{54}Fe (n,γ)^{55}Fe	^{54}Fe (n,p)^{54}Mn
	^{62}Ni (n,γ)^{63}Ni	^{54}Fe (n,d)^{53}Mn
		^{60}Ni (n,p)^{60}Co
Copper		^{63}Cu (n,p)^{63}Ni
		^{63}Cu (n,α)^{60}Co
$PbWO_4$	^{180}W (n,γ)^{181}W	
	^{204}Pb (n,γ)^{205}Pb	
MGN-Concrete	^{40}Ca (n,γ)^{41}Ca	^{54}Fe (n,p)^{54}Mn
Concrete	^{44}Ca (n,γ)^{45}Ca	^{54}Fe (n,d)^{53}Mn
	^{54}Fe (n,γ)^{55}Fe	
Pb, Pb-polyconc.	^{204}Pb (n,γ)^{205}Pb	

Table 2: Materials where neutron reactions have been considered and list of the reactions taken into account.

$\phi = 10^3$ cm^{-2}s^{-1} this implies that one weight percent of cobalt would lead to a ^{60}Co-activity of about 1 Bq/g.

In addition to the effects due to impurities and unknown material compositions some neutron activation reactions (e.g. ^{204}Pb(n,p)^{204}Tl) could not be taken into account since no cross section data were available. None of the reactions omitted for this reason are expected to be very significant.

2.6 Follow-up of the time dependence

We use the DETRA [7] code to follow the time dependence of the activation. DETRA uses an up-to-date radionuclide library with complete decay chain information and solves the differential equations describing the time development of an arbitrary set of radionuclides taking into account different production and transmutation processes.

In cases where unknown nuclides are in the residual nuclide output of FLUKA – which happens rarely due to the completeness of the library – DETRA sets the decay time to zero and produces one 800 keV photon per decay. The decay mode in such cases is β-decay towards the stability line.

DETRA allows us to follow exactly the assumed LHC-irradiation schedule and subsequent decay up to arbitrarily long cooling times. We do the DETRA calculations for high-energy activation, thermal neutron activation and fast neutron activation and for each of the 9 CMS materials. In total this gives us 19 times dependence curves for activity [2)] and another 19 for the energy emission. Under the assumptions described above these curves have a universal shape, and thus can be scaled with any star production rate or neutron flux to give the activity at a given location in CMS at any instant of time.

3 Results

Fig. 1 shows the time dependence of the activity for 9 different materials in CMS due to high-energy hadronic interactions. This data is scaled so that the curves give the activity (or energy emitted) per unit

[2)] not 27, since some materials have no important neutron activation channels

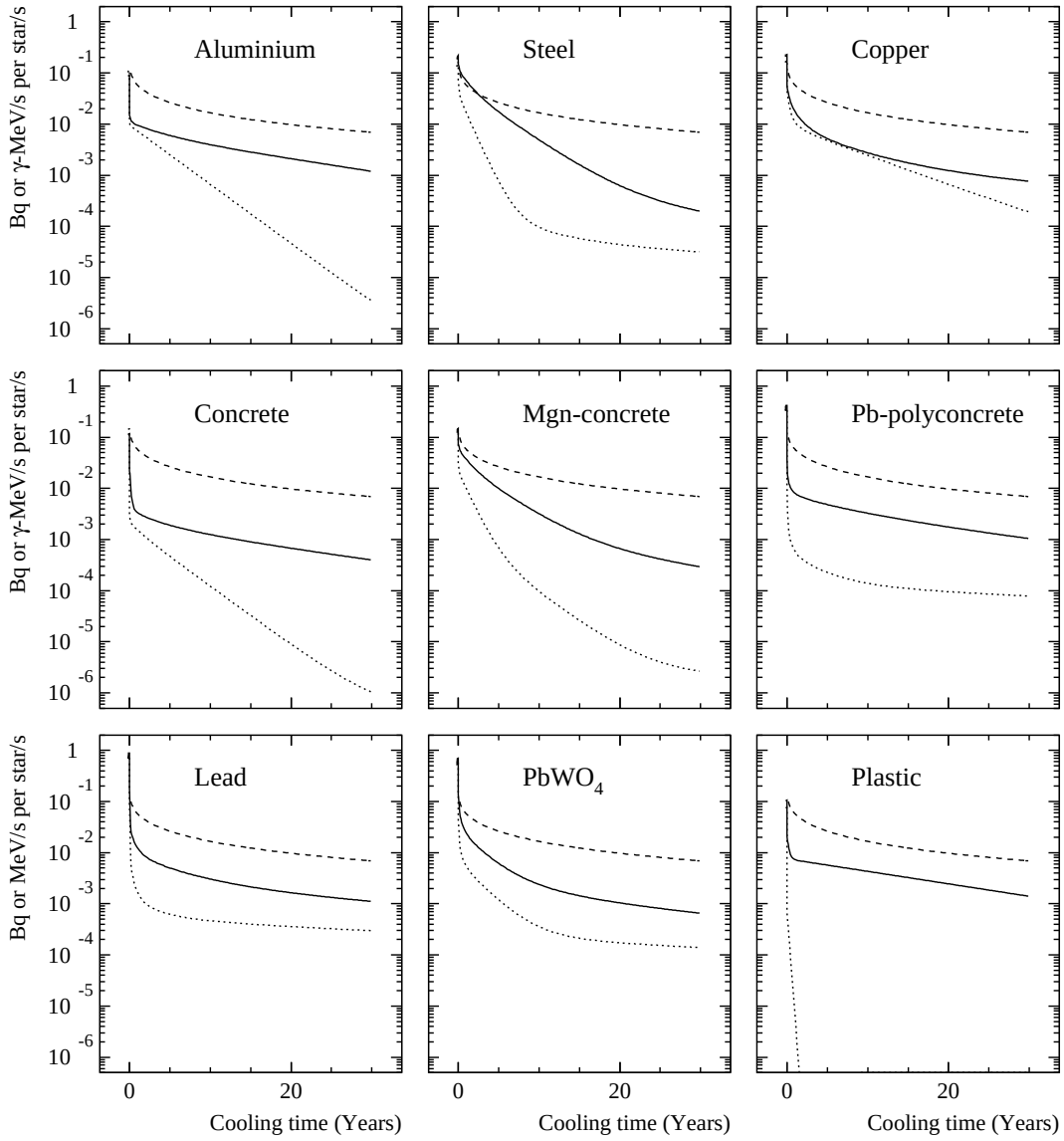

Figure 1: Time dependence of activity for the most important CMS materials due to high-energy hadronic interactions. The curves correspond to 10 years irradiation with the assumed luminosity profile and are normalized with star densities at LHC peak luminosity. Solid line=Activity, Dotted line = γ-energy, dashed line = Overton-Sullivan with 'Bq'/star = 0.33, corresponding to the previous study [1].

of star density at LHC peak luminosity. The luminosity profile, as explained in section 2.1 has been taken into account when calculating the curves of Fig. 1. Thus the curves are specific to the LHC irradiation and cannot be applied to any other case. In addition they correspond to the activity decay after 10 years of LHC operation.

Three curves are shown in each case. One pair of curves corresponds to the FLUKA/DETRA simulation results for activity (Bq) and energy emission as photons (γ-MeV/s). The third curve shows the Overton-Sullivan formula with the universal 'Bq'/star factor of 0.33. This corresponds to the assumption made in the previous study [1]. The total activities (energy emission rates) and three most important nuclides can

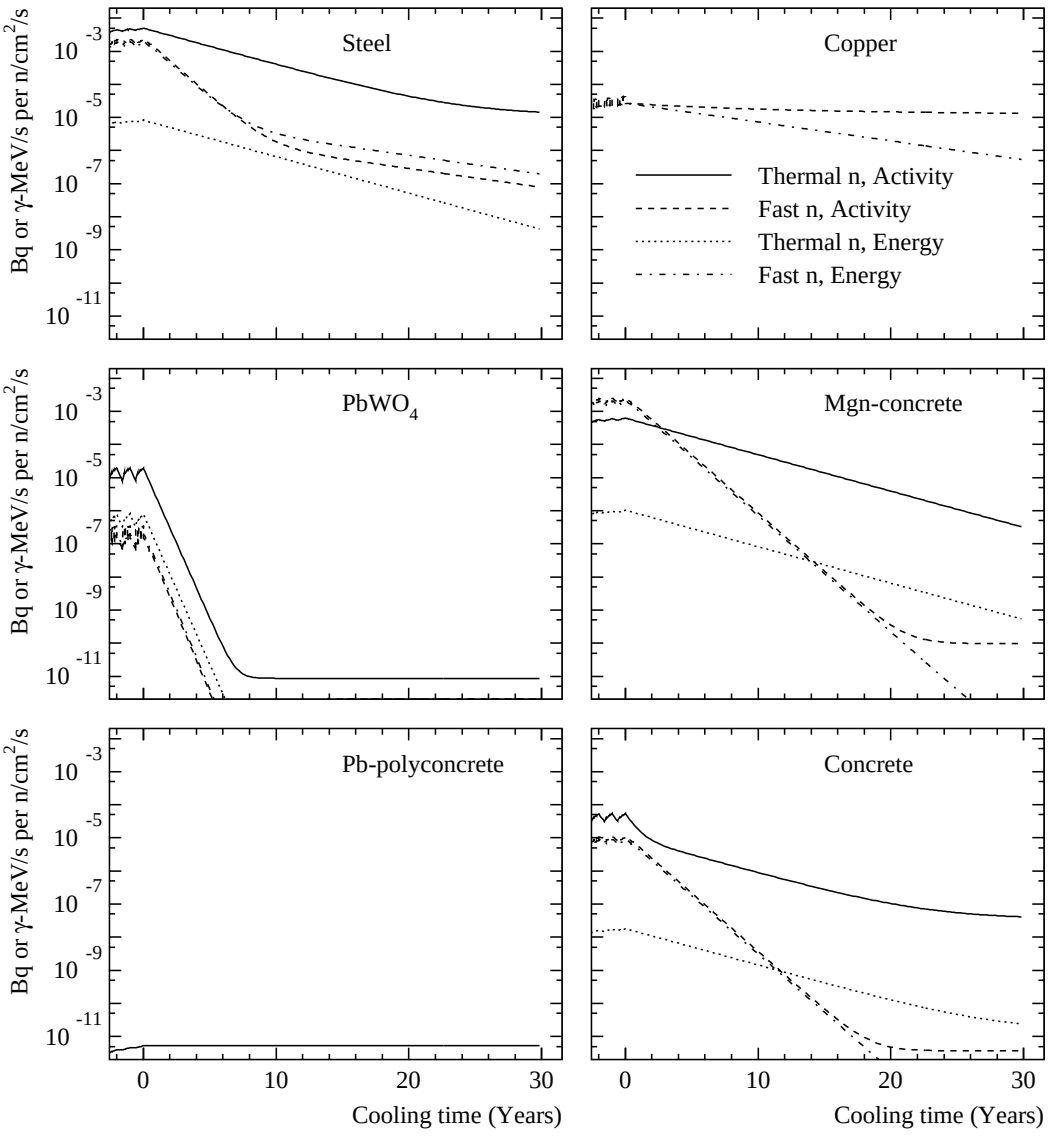

Figure 2: Time dependence of activity for the most important CMS materials due to low-energy neutron interactions. The curves correspond to 10 years irradiation with the assumed luminosity profile and are normalized with neutron fluxes at LHC peak luminosity.

be found in Tables 4 and 5 of appendix A. A comparison of these two tables reveals that in most cases the nuclides responsible for most of the activity do not contribute significantly to the emitted energy. In particular the large activities of the two radiologically almost harmless nuclides, tritium and ^{55}Fe, should be noted.

Fig. 2 shows the corresponding activation from thermal and fast neutrons. Again we show both the activity and the emitted gamma energy. In addition we have to make a distinction between thermal and fast neutrons. Thus for each material two or four curves are shown, depending on the existence of activation channels. For aluminium and plastic no significant neutron activation is expected and neutron activation of pure lead will be comparable the Pb-polyconcrete. Like the curves in Fig. 1, also those of

Fig. 2 are valid only for the assumed LHC luminosity profile and are normalized to the corresponding neutron fluxes at peak luminosity.

With the information contained in Figs. 1 and 2 and the star density and neutron fluence binnings from FLUKA simulations we can estimate the radionuclide yields and the time development of the activity.

The radioactive material will be classified in terms of activity per unit of mass. This poses two problems which make a presentation of the data difficult

1. In a complicated and large system like CMS the activities will have a strong spatial variation. Thus the total volume of steel falling into a given activity category might be embedded in several natural components of CMS. One might not be willing to start cutting the CMS steel and other elements into pieces in order to separate the material according to its activation.

2. Activity is by no means directly related to the radiological danger. The only way to assess correctly activation would be to list the radioisotopes individually. For CMS, where we have to deal with tens of individual volumes this would lead to an amount of data which cannot be presented in any reasonable way.

The solutions we have chosen for these two problems are

1. We present the data both in terms of total amount of material in a given activity category independent of where the material is located. In addition we present the average activity for the main components of CMS.

2. We present the activity in Bq/g no matter what kind of decay. This puts for instance ^{55}Fe and ^{60}Co on the same footing, even though their radiological dangers are very different. To assess the radiological danger from bulk objects better we present also the total energy of photons emitted per unit of time per unit of mass. This gives a good feeling of the radiological danger of bulk objects, since the mass absorption coefficient in tissue is almost constant over the interesting γ-energy range. This also is equivalent to the definition of ω-factors (see appendix B), although our approach is much more detailed and allows a detailed follow-up of the time-dependence. The radiological implications of β-emitters are not considered by this, but they are less important for bulk material than for thin layers, gases or aerosols. None of the latter is significant for this study.

The masses of different CMS components and materials are obtained from the FLUKA simulation geometry. Thus they will not correspond to the actual engineering masses of CMS, but only approximate them.

Table 6 (appendix A) shows the amount of material of a given kind in each of the three activity categories. These data do not include any correlation with the actual distribution of the material, i.e. in most cases the amount with the indicated activity will be mixed with material from different categories. In addition to classifying the material according to the activity and the γ-energy emission rate, we show a third column with the prediction corresponding to the assumptions of Ref. [1].

The observations to be made are that the γ-energy emission rates are systematically lower than the activities. A small difference is explained by the scaling to 1 MeV as opposed to few hundred keV on average per decay. For steel and copper the difference between the two definitions is not very large, whereas it is significant for plastic and all concretes. This is explained by the dominance of tritium, which contributes significantly to the activity but does not emit photons. A general trend for most materials seems to be that the average γ-energy per Bq decreases with increasing cooling time.

t_c	1-10 Bq/g	10-100 Bq/g	>100 Bq/g	1-10 γ-MeV/g/s	10-100 γ-MeV/g/s	>100 γ-MeV/g/s	1-10 'Bq'/g	10-100 'Bq'/g	>100 'Bq'/g
	Estimated Amount of Active Material								
0.1 a	**609.5**	**663.4**	**365.2**	683.2	534.7	299.3	880.4	601.7	263.9
1 a	**611.3**	**502.4**	**278.1**	613.0	393.7	211.0	860.4	440.9	189.3
10 a	**382.5**	**146.5**	**39.8**	157.8	24.5	4.0	684.4	230.6	87.8
20 a	**205.2**	**46.4**	**6.1**	66.4	4.1	3.4	558.9	182.9	60.0
30 a	**133.5**	**13.8**	**3.8**	31.2	2.5	2.0	474.2	162.9	43.9
	Averaged by CMS Region								
0.1 a	2430.9	398.1	693.6	1923.7	663.1	351.2			
1 a	1919.5	667.3	351.2	786.5	515.2	351.2			
10 a	404.5	290.7	4.2	288.2	0.2	4.0			
20 a	382.5	0.2	4.0	128.1	0.0	4.0			
30 a	322.1	0.2	4.0	0.2	0.0	4.0			

Table 3: Total amount (tons) of active material in each category after 10 years LHC operation and the indicated cooling time. The upper part of the table gives the sum over Table 6 and the lower part is the sum over Table 8. The numbers include the collimators and all the surrounding shielding, but not the cavern walls.

The comparison to the ω-factors and the Overton-Sullivan formula shows large discrepancies which increase with increasing cooling time. In particular the amount of material in the most active category after 30 years of cooling is found to be 40 t if these crude parametrizations are used. While this value is in perfect agreement with [1], the new more detailed and realistic calculations show less than 4 tons in this category after 30 years of cooling.

These large differences clearly call for an explanation. Apparently something is wrong with the ω-factors but to a larger extent with the Overton-Sullivan formula, which predicts a too slow decay of the induced radioactivity. A detailed discussion can be found in appendix B.

Table 7 (appendix A) gives one indication of the importance of low-energy neutron activation as a function of cooling time by giving the total amount of material in all categories (>1 Bq/g) for high-energy activation only and with low-energy neutron activation added.

Table 8 (appendix A) gives a different assessment of the activation by identifying natural components within CMS and giving their average activation. Again different cooling times are considered. Also the activities and γ-energy emission rates are considered separately. The high-energy activation is again shown alone and together with the low-energy neutron activation. A comparison seems to indicate a larger effect from the low-energy neutrons than found Table 7. Such a comparison between the two tables, however, is very difficult because they are constructed in quite a different way. While Table 7 shows data which are obtained in small spatial bins considering both the neutron and high-energy flux in that bin only, Table 8 shows the sums of the averages over large volumes. In general the neutron flux will be more uniform than the high-energy flux, so neutron activation becomes more important with respect to the high-energy activation when averaging is done over a large volume. Also, Table 7 shows only the material with activity above 1 Bq/g (1 γ-MeV/g/s, respectively). Most of the differences seen in Table 8 will not show up in this simple comparison, because the material, will fall into the same category whether the neutron activation is considered or not.

Table 3 shows the final result of this study in the most compressed form possible by displaying the

estimates of the amount of activated material in CMS for several cooling times. We feel that we have to present the results for all discussed estimation methods, using both the activity and the energy emission rate as classification criteria. As can be seen, the differences are significant. The rightmost columns in the upper table give only a cross check to the old study. We consider the middle column in the upper table as the update to this result. The corresponding leftmost upper table gives the estimates of total activities.

The lower part of the table gives corresponding values but under the assumption that none of the CMS components would be cut into pieces to separate material of different activity.

The truth probably lies somewhere in between the two approaches; it is unlikely that the Yoke would be cut into pieces, but the calorimeters, for instance, can quite naturally be disassembled into small elements. Since most of the highly active parts are found in the calorimeters, the upper part of Table 3 might be closer to reality. Considering the activities, shown in bold, we observe that 30 years after LHC shutdown we will be left with about 150 tons of material which is considered radioactive. However, only 4 tons are in the highest category and in fact all this activation is located in the collimators, which should be counted as machine elements and have been included in this study only for completeness.

Although the initial amount of active material agrees fairly well with the previous study [1], the reduction from the former estimate at long cooling times is significant: a factor of 4 in the total amount of active material and an order of magnitude for material in the highest activity category. And if the energy emission rates are compared, which in fact is be more appropriate, the difference is even larger. These large differences are discussed in detail in appendix B. There is sufficient evidence for a failure of the Overton-Sullivan formula at long cooling times, so that the new estimates should be considered more reliable.

4 Summary

We have described a new method to estimate the residual activity and dose rate in materials activated at hadron accelerators. Our approach consists of an explicit calculation of individual isotope yields. But in order to collect sufficient statistics we still maintain some of the classical concept to parametrize activation with star densities. The major improvement is that instead of the dose, we parametrize the radionuclide yields as a function of the star density and/or neutron flux. The latter is divided into the thermal flux and the flux above 1 MeV. This value is set by the actual thresholds of the reactions considered, which in this case are around a few MeV.

Having established complete inventories of the radioisotopes we are able to follow the time dependence accurately, allowing us to extract a complete γ-spectrum at any instant of time.

We have shown that our method agrees well with the classical ω-factors and the Overton-Sullivan parametrization of the time dependence in the range where the latter is valid. We give arguments why our method should be more accurate for long cooling and irradiation times.

The estimate for the amount of active material left over from CMS after 30 years of cooling is significantly reduced by the new calculations. We now estimate to have 150 tons of active material (>1 Bq/g) 30 years after LHC-shutdown. Only the copper collimators (4 tons in total), which actually are counted as machine elements, will fall into the highest activity category after 30 years of cooling.

References

[1] M. Huhtinen, CERN CMS IN 1997/006 (1997).

[2] J. Ranft and K. Goebel, CERN HP-70-92 (1970).

[3] R. Thomas and G. Stevenson, *Radiological Safety Aspects of the Operation of Proton Accelerators*, Technical Report Series No 283, IAEA Vienna (1988)

[4] A. Sullivan and T. Overton, Health Physics 11 (1965) 1101.

[5] A. Iljinov *et al., Production of Radionuclides at Intermediate Energies,* Landolt-Börnstein, New Series Vols 13a-e, ed. H. Schopper, Springer (1991-1993).

[6] P. A. Aarnio *et al*, CERN TIS-RP/168 (1986) and CERN TIS-RP/190 (1987)
A. Fassò *et al*, Proc IV Int. Conf. on Calorimetry in High Energy Physics, La Biodola, Sept 20-25, 1993, Ed. A. Menzione and A. Scribano, World Scientific, p. 493 (1993).
A. Fassò *at al*, Specialists' Meeting on Shielding Aspects of Accelerators, Targets and Irradiation Facilities. Arlington, Texas, April 28-29, 1994. NEA/OECD doc. p. 287 (1995).

[7] P. A. Aarnio, CERN CMS Note, in preparation.

A Tables of radionuclide yields and activities

Tables 4 and 5 list the radionuclide yields in high-energy reactions. The top three isotopes are indicated for different cooling times after an irradiation which corresponds to 10 years of LHC operation. Table 4 gives the values with respect to activity (Bq) while Table 5 refers to the γ-energy emission rate. A comparison shows significant differences for most materials.

Table 6 gives the estimated total amount of activated materials in the different categories. These data are independent of where the material is located. In most cases it will be mixed with material from another activity category. Table 6 shows the amount of active material if the activity or γ-energy emission rate are used as the criterium. In addition the prediction corresponding to the assumptions made in a previous work is shown, but based on the new simulation geometry.

Table 7 shows the total amount of material with specific activity above 1 Bq/g (or 1 γ-MeV/g/s, respectively) with and without consideration of low-energy neutron activation.

Table 8 shows the average activity of several natural CMS components. The difference to Table 6 is that here it is assumed that these natural entities would not be cut or disassembled in order to separate pieces falling into different categories.

	Aluminium	Steel	Copper	Concrete	MGN-Concrete	Pb-polyconcrete	Lead	$PbWO_4$	Plastic
0	0.090 Bq	0.22 Bq	0.23 Bq	0.12 Bq	0.15 Bq	0.42 Bq	0.89 Bq	0.71 Bq	0.11 Bq
	^{26m}Al (25.5)	^{55}Fe (25.7)	^{62}Cu (23.9)	^{15}O (28.1)	^{55}Fe (20.0)	^{18}F (6.5)	^{203}Pb (5.2)	^{203}Pb (3.3)	^{11}C (56.4)
	^{24}Na (8.9)	^{54}Mn (19.5)	^{61}Cu (16.3)	^{37}Ar (10.5)	^{15}O (17.0)	^{203}Pb (6.4)	^{201}Tl (4.1)	^{179}W (2.5)	^{7}Be (13.6)
	^{18}F (8.2)	^{51}Cr (13.2)	^{64}Cu (13.4)	^{11}C (9.9)	^{54}Mn (16.4)	^{201}Tl (4.4)	^{204m}Pb (3.5)	^{181}W (2.5)	^{12}Be (10.0)
1 d	0.017 Bq	0.16 Bq	0.072 Bq	0.022 Bq	0.079 Bq	0.11 Bq	0.25 Bq	0.24 Bq	0.022 Bq
	^{3}H (38.2)	^{55}Fe (34.2)	^{58}Co (25.1)	^{37}Ar (54.4)	^{55}Fe (37.0)	^{203}Pb (18.5)	^{203}Pb (13.8)	^{181}W (7.1)	^{7}Be (65.7)
	^{22}Na (25.8)	^{54}Mn (25.9)	^{57}Co (18.5)	^{7}Be (12.3)	^{54}Mn (30.2)	^{201}Tl (14.8)	^{201}Tl (12.5)	^{203}Pb (6.9)	^{3}H (34.4)
	^{7}Be (20.3)	^{51}Cr (17.0)	^{64}Cu (11.7)	^{3}H (8.6)	^{51}Cr (14.3)	^{200}Tl (10.5)	^{200}Tl (8.9)	^{178m}Hf (5.7)	^{14}C (<0.1)
7 d	0.014 Bq	0.15 Bq	0.056 Bq	0.020 Bq	0.074 Bq	0.038 Bq	0.087 Bq	0.14 Bq	0.021 Bq
	^{3}H (46.2)	^{55}Fe (37.2)	^{58}Co (30.5)	^{37}Ar (54.9)	^{55}Fe (39.4)	^{202}Tl (13.8)	^{202}Tl (11.2)	^{181}W (12.4)	^{7}Be (63.9)
	^{22}Na (31.1)	^{54}Mn (27.9)	^{57}Co (23.5)	^{7}Be (12.9)	^{54}Mn (31.9)	^{3}H (11.7)	^{195}Au (10.8)	^{179}Ta (8.8)	^{3}H (36.1)
	^{7}Be (22.7)	^{51}Cr (16.0)	^{55}Fe (8.9)	^{3}H (9.8)	^{51}Cr (13.1)	^{201}Tl (10.7)	^{201}Tl (9.2)	^{178m}Hf (8.5)	^{14}C (<0.1)
30 d	0.013 Bq	0.13 Bq	0.048 Bq	0.014 Bq	0.065 Bq	0.019 Bq	0.038 Bq	0.084 Bq	0.017 Bq
	^{3}H (49.3)	^{55}Fe (42.7)	^{58}Co (28.6)	^{37}Ar (49.3)	^{55}Fe (44.3)	^{3}H (23.9)	^{195}Au (22.4)	^{181}W (17.6)	^{7}Be (56.8)
	^{22}Na (32.7)	^{54}Mn (31.0)	^{57}Co (26.0)	^{3}H (13.8)	^{54}Mn (34.6)	^{204}Tl (13.7)	^{204}Tl (12.6)	^{179}Ta (13.8)	^{3}H (43.2)
	^{7}Be (18.0)	^{51}Cr (10.5)	^{55}Fe (10.3)	^{7}Be (13.5)	^{51}Cr (8.5)	^{195}Au (13.6)	^{202}Tl (6.9)	^{175}Hf (7.0)	^{14}C (<0.1)
1 a	0.0095 Bq	0.073 Bq	0.018 Bq	0.0034 Bq	0.038 Bq	0.0082 Bq	0.013 Bq	0.025 Bq	0.0074 Bq
	^{3}H (63.9)	^{55}Fe (61.0)	^{57}Co (30.7)	^{3}H (53.9)	^{55}Fe (61.0)	^{3}H (52.0)	^{204}Tl (32.1)	^{179}Ta (33.3)	^{3}H (97.5)
	^{22}Na (35.6)	^{54}Mn (27.7)	^{55}Fe (21.4)	^{22}Na (18.3)	^{54}Mn (29.8)	^{204}Tl (26.8)	^{195}Au (21.3)	^{181}W (10.1)	^{7}Be (2.5)
	^{7}Be (0.5)	^{49}V (8.1)	^{60}Co (17.3)	^{55}Fe (15.2)	^{49}V (4.3)	^{195}Au (9.9)	^{3}H (16.7)	^{173}Lu (8.7)	^{14}C (<0.1)
10 a	0.0040 Bq	0.0052 Bq	0.0028 Bq	0.0013 Bq	0.0033 Bq	0.0033 Bq	0.0031 Bq	0.0025 Bq	0.0044 Bq
	^{3}H (92.0)	^{55}Fe (90.3)	^{60}Co (35.4)	^{3}H (87.8)	^{55}Fe (73.3)	^{3}H (78.4)	^{3}H (42.1)	^{3}H (47.2)	^{3}H (100)
	^{22}Na (7.9)	^{3}H (8.1)	^{3}H (33.7)	^{22}Na (4.6)	^{3}H (24.8)	^{204}Tl (13.1)	^{204}Tl (26.2)	^{204}Tl (15.7)	^{14}C (<0.1)
	^{14}C (0.03)	^{44}Sc (0.3)	^{63}Ni (14.9)	^{55}Fe (4.3)	^{22}Na (1.2)	^{193}Pt (4.3)	^{193}Pt (13.9)	^{179}Ta (11.7)	^{10}Be (<0.1)
30 a	0.0012 Bq	0.00020 Bq	0.00077 Bq	0.00041 Bq	0.0003 Bq	0.0011 Bq	0.0011 Bq	0.00067 Bq	0.0014 Bq
	^{3}H (99.8)	^{3}H (67.2)	^{63}Ni (46.9)	^{3}H (90.2)	^{3}H (91.0)	^{3}H (80.4)	^{3}H (38.0)	^{3}H (57.6)	^{3}H (100)
	^{22}Na (0.1)	^{55}Fe (15.3)	^{3}H (40.3)	^{39}Ar (7.9)	^{55}Fe (5.5)	^{193}Pt (10.1)	^{193}Pt (28.9)	^{193}Pt (17.2)	^{14}C (<0.1)
	^{14}C (0.1)	^{44}Sc (6.2)	^{60}Co (9.6)	^{14}C (1.1)	^{39}Ar (1.6)	^{207}Bi (1.9)	^{207}Bi (6.7)	^{207}Bi (3.4)	^{10}Be (<0.1)

Table 4: Residual nuclide activities in 9 materials present at CMS as a function of cooling time. The values are given normalized to one star per second at LHC peak luminosity. The values in parentheses give the proportion of the indicated nuclide with respect to the total activity.

	Aluminium	Steel	Copper	Concrete	MGN-Concrete	Pb-polyconcrete	Lead	$PbWO_4$	Plastic
0	110 keV	170 keV	180 keV	150 keV	140 keV	370 keV	790 keV	610 keV	75 keV
	^{24}Na (29.1)	^{54}Mn (21.1)	^{62}Cu (31.4)	^{15}O (23.2)	^{15}O (18.7)	^{204m}Pb (10.3)	^{204m}Pb (8.5)	^{171}Hf (12.2)	^{11}C (81.8)
	^{26m}Al (20.7)	^{52}Mn (14.3)	^{61}Cu (17.7)	^{38}K (15.5)	^{54}Mn (14.7)	^{18}F (7.6)	^{200}Tl (5.1)	^{204m}Pb (5.4)	^{11}Be (8.7)
	^{22}Na (8.4)	^{48}V (10.7)	^{58}Co (10.1)	^{16}N (11.5)	^{16}N (9.9)	^{200}Tl (5.5)	^{198}Tl (4.5)	^{176}Ta (4.1)	^{15}O (2.5)
1 d	20 keV	91 keV	55 keV	4.4 keV	39 keV	48 keV	130 keV	120 keV	0.73 keV
	^{24}Na (52.9)	^{54}Mn (39.0)	^{58}Co (32.1)	^{22}Na (39.5)	^{54}Mn (51.5)	^{200}Tl (30.4)	^{200}Tl (22.2)	^{171}Hf (15.4)	^{7}Be (100)
	^{22}Na (46.3)	^{52}Mn (23.4)	^{56}Co (18.3)	^{24}Na (30.1)	^{52}Mn (27.8)	^{203}Pb (12.8)	^{188}Ir (8.3)	^{178m}Hf (11.2)	^{18}F (<0.1)
	^{7}Be (0.83)	^{48}V (19.0)	^{60}Co (16.4)	^{54}Mn (10.2)	^{48}V (10.0)	^{202}Tl (7.2)	^{203}Pb (8.3)	^{200}Tl (10.6)	—
7 d	9.6 keV	70 keV	46 keV	2.6 keV	31 keV	13 keV	39 keV	45 keV	0.67 keV
	^{22}Na (98.2)	^{54}Mn (50.2)	^{58}Co (36.3)	^{22}Na (66.7)	^{54}Mn (64.1)	^{202}Tl (19.7)	^{188}Ir (20.4)	^{178m}Hf (25.6)	^{7}Be (100)
	^{7}Be (1.6)	^{48}V (19.2)	^{56}Co (20.9)	^{54}Mn (17.2)	^{52}Mn (16.7)	^{188}Ir (16.3)	^{205}Bi (14.4)	^{172}Lu (11.8)	—
	^{24}Na (0.1)	^{52}Mn (14.5)	^{60}Co (19.6)	^{7}Be (4.9)	^{48}V (9.7)	^{205}Bi (11.4)	^{206}Bi (12.7)	^{182}Ta (7.4)	—
30 d	9.4 keV	47 keV	37 keV	2.3 keV	23 keV	3.7 keV	12 keV	23 keV	0.50 keV
	^{22}Na (98.8)	^{54}Mn (70.1)	^{58}Co (36.0)	^{22}Na (74.1)	^{54}Mn (82.9)	^{202}Tl (18.0)	^{205}Bi (15.8)	^{178m}Hf (23.7)	^{7}Be (100)
	^{7}Be (1.3)	^{56}Co (11.2)	^{60}Co (24.2)	^{54}Mn (18.4)	^{22}Na (5.2)	^{205}Bi (13.5)	^{188}Ir (13.6)	^{172}Lu (21.5)	—
	^{26}Al (<0.1)	^{48}V (10.4)	^{56}Co (21.1)	^{7}Be (4.1)	^{48}V (4.9)	^{188}Ir (11.7)	^{185}Os (11.0)	^{182}Ta (12.4)	—
1 a	7.4 keV	18 keV	11 keV	1.6 keV	11 keV	0.62 keV	1.8 keV	5.7 keV	0.0092 keV
	^{22}Na (100)	^{54}Mn (94.7)	^{60}Co (69.9)	^{22}Na (86.1)	^{54}Mn (90.0)	^{22}Na (38.4)	^{172}Lu (19.2)	^{172}Lu (64.1)	^{7}Be (100)
	^{7}Be (<0.1)	^{56}Co (1.9)	^{54}Mn (12.2)	^{54}Mn (13.5)	^{22}Na (9.0)	^{195}Au (11.5)	^{195}Au (13.3)	^{182}Ta (7.9)	—
	^{26}Al (<0.1)	^{57}Co (0.9)	^{57}Co (6.2)	^{7}Be (0.1)	^{56}Co (0.5)	^{207}Bi (9.6)	^{207}Bi (12.3)	^{173}Lu (6.4)	—
10 a	0.70 keV	0.10 keV	2.5 keV	0.13 keV	0.10 keV	0.14 keV	0.47 keV	0.37 keV	0.0 MeV
	^{22}Na (100)	^{60}Co (38.5)	^{60}Co (99.0)	^{22}Na (99.3)	^{22}Na (86.3)	^{207}Bi (34.4)	^{207}Bi (38.3)	^{172}Lu (36.7)	—
	^{26}Al (<0.1)	^{44}Sc (35.8)	^{44}Sc (0.7)	^{42}K (0.3)	^{54}Mn (6.9)	^{207m}Pb (30.3)	^{207m}Pb (33.7)	^{207}Bi (14.6)	—
	—	^{54}Mn (12.7)	^{22}Na (0.1)	^{54}Mn (0.1)	^{55}Fe (3.9)	^{22}Na (15.8)	^{194}Au (15.6)	^{178n}Hf (14.4)	—
30 a	0.0038 keV	0.032 keV	0.20 keV	0.0011 keV	0.0027 keV	0.079 keV	0.30 MeV	0.14 keV	0.0 MeV
	^{22}Na (93.8)	^{44}Sc (84.2)	^{60}Co (92.7)	^{22}Na (60.3)	^{44}Sc (74.8)	^{207}Bi (39.9)	^{207}Bi (38.9)	^{207}Bi (25.0)	—
	^{26}Al (6.2)	^{60}Co (9.0)	^{44}Sc (6.5)	^{42}K (23.3)	^{22}Na (17.1)	^{207m}Pb (35.1)	^{207m}Pb (34.2)	^{178n}Hf (24.5)	—
	—	^{44}Ti (5.5)	^{44}Ti (0.4)	^{44}Sc (9.8)	^{44}Ti (4.9)	^{194}Au (22.2)	^{194}Au (23.8)	^{207m}Pb (22.0)	—

Table 5: Residual nuclide total γ-energies in 9 materials present at CMS as a function of cooling time. The values are normalized to one star per second at LHC peak luminosity. The values in parentheses give the proportion of the indicated nuclide with respect to the total emitted γ-energy.

t_c	1-10 Bq/g	10-100 Bq/g	>100 Bq/g	1-10 γ-MeV/g/s	10-100 γ-MeV/g/s	>100 γ-MeV/g/s	1-10 'Bq'/g	10-100 'Bq'/g	>100 'Bq'/g
Aluminium, total estimated mass: 412 t									
30 d	1.7	1.5	0.3	1.9	1.4	0.2	—	1.7	1.7
1 a	1.9	1.4	0.2	2.1	1.2	0.1	—	2.3	1.2
10 a	2.5	0.8	0.1	1.1	0.1	—	1.4	1.6	0.4
20 a	2.0	0.5	—	0.1	—	—	1.9	1.4	0.2
30 a	1.5	0.3	—	—	—	—	2.2	1.1	0.1
Steel, total estimated mass: 10836 t									
30 d	210.6	333.7	299.5	230.7	306.4	258.1	301.0	246.4	209.5
1 a	236.2	298.4	253.6	304.8	234.3	198.5	339.2	192.6	161.3
10 a	244.3	134.6	35.6	107.0	21.5	—	285.4	157.3	79.4
20 a	142.3	42.1	2.1	50.2	3.5	—	230.6	142.0	54.0
30 a	89.3	12.1	—	27.9	0.5	—	199.7	135.2	39.3
Copper, total estimated mass: 1389 t (incl. absorbers $\approx$ 4 t)									
30 d	272.9	60.0	12.0	235.9	51.3	9.3	417.4	97.1	25.6
1 a	142.0	34.1	5.1	103.0	23.9	4.0	308.8	65.1	14.4
10 a	51.9	5.0	4.0	44.3	2.9	4.0	124.2	31.1	4.6
20 a	36.0	0.9	4.0	13.7	0.6	3.4	86.6	18.7	4.0
30 a	29.3	0.2	3.8	1.6	2.0	2.0	71.1	12.0	4.0
$PbWO_4$, total estimated mass: 101 t									
30 d	5.8	85.2	9.7	82.1	15.2	3.3	0.3	88.3	12.1
1 a	81.1	16.1	3.5	64.5	7.6	—	23.9	69.1	7.6
10 a	15.4	3.5	—	5.1	—	—	85.2	13.3	2.1
20 a	10.1	1.1	—	2.2	—	—	87.2	10.1	1.0
30 a	8.3	0.1	—	1.6	—	—	76.7	8.3	0.1
Magnetite concrete, total estimated mass: 309 t									
30 d	94.8	170.3	42.1	113.1	159.4	28.4	125.8	140.3	9.2
1 a	124.5	148.4	15.2	137.5	126.7	8.4	163.1	86.8	1.1
10 a	47.6	—	—	—	—	—	162.7	16.5	—
20 a	2.8	—	—	—	—	—	125.9	6.4	—
30 a	—	—	—	—	—	—	99.2	2.7	—
Lead-loaded polyconcrete, total estimated mass: 30 t									
30 d	9.9	4.4	1.4	2.8	0.2	—	12.2	7.6	4.5
1 a	5.0	3.2	0.5	—	—	—	14.0	5.2	3.3
10 a	5.0	2.5	0.1	—	—	—	9.8	4.4	1.3
20 a	4.6	1.8	—	—	—	—	6.0	3.5	0.8
30 a	4.0	1.1	—	—	—	—	5.1	3.1	0.4
Lead, total estimated mass: 1.2 t									
30 d	—	1.0	0.2	0.4	0.8	—	—	0.4	0.8
1 a	0.4	0.8	—	1.1	—	—	—	0.8	0.4
10 a	1.1	0.1	—	0.3	—	—	0.2	1.0	—
20 a	1.0	—	—	0.2	—	—	0.6	0.7	—
30 a	0.8	—	—	0.1	—	—	0.7	0.5	—
Plastic, total estimated mass: 70 t (cables not included)									
30 d	13.8	7.3	—	16.3	—	—	23.7	19.9	0.5
1 a	20.2	—	—	—	—	—	11.4	19.0	—
10 a	14.7	—	—	—	—	—	15.5	5.4	—
20 a	6.4	—	—	—	—	—	20.1	0.1	—
30 a	0.3	—	—	—	—	—	19.5	—	—
Concrete, total estimated mass: 6294 t (cavern walls and block house)									
30 d	149.0	27.2	—	65.9	—	—	290.2	135.7	17.2
1 a	74.7	—	—	42.7	—	—	240.6	98.5	2.4
10 a	20.6	—	—	—	—	—	155.1	31.6	—
20 a	4.0	—	—	—	—	—	125.7	12.1	—
30 a	—	—	—	—	—	—	108.1	4.5	—

Table 6: Amount of radioactive material in the CMS area (tons) for different cooling times. The last columns provide the comparison to the previous study [1], where a 'Bq' is defined as the emission of one 800 keV photon.

t_c	Activity		Energy emission rate	
	Total	HE only	Total	HE only
	Steel			
0.1 a	843.8	764.5	795.2	666.1
1.0 a	788.2	716.3	737.6	531.7
10.0 a	414.5	334.8	128.5	53.9
20.0 a	186.5	165.5	53.7	25.1
29.9 a	101.4	88.9	28.4	18.7
	Copper			
0.1 a	344.9	340.9	296.5	285.6
1.0 a	181.2	172.2	130.9	120.7
10.0 a	60.9	49.5	51.2	44.6
20.0 a	40.9	27.5	17.7	15.8
29.9 a	33.3	17.7	5.6	5.1
	$PbWO_4$			
0.1 a	100.7	100.7	100.6	100.6
1.0 a	100.7	100.7	72.1	72.1
10.0 a	18.9	18.9	5.1	5.1
20.0 a	11.2	11.2	2.2	2.2
29.9 a	8.4	8.4	1.6	1.6
	Magnetite Concrete			
0.1 a	307.2	252.4	300.9	200.6
1.0 a	288.1	234.2	272.6	140.1
10.0 a	47.6	43.8	0.0	0.0
20.0 a	2.8	2.2	0.0	0.0
29.9 a	0.0	0.0	0.0	0.0
	Concrete			
0.1 a	229.0	170.0	65.9	45.5
1.0 a	139.8	65.4	42.7	29.1
10.0 a	49.0	20.6	0.0	0.0
20.0 a	7.5	4.0	0.0	0.0
29.9 a	0.0	0.0	0.0	0.0

Table 7: Total amount of active material (tons) in categories 1-3 for the five material types with significant neutron activation. The comparison serves to indicate the role of neutron activation, taken into account in the 'Total' but not in the 'HE only' numbers.

	Bq/g		γ-MeV/g/s		Bq/g		γ-MeV/g/s	
t_i	HE	Total	HE	Total	HE	Total	HE	Total
	Tracker (1.2 t)				YE1 (1500 t)			
1 a	25.00	25.00	1.80	1.80	0.17	0.07	0.09	0.02
10 a	14.00	14.00	0.16	0.16	0.01	—	—	—
30 a	4.60	4.60	—	—	—	—	—	—
	ECAL Moderators (3.0 t)				YE2 (1400 t)			
1 a	24.00	24.00	0.03	0.03	0.22	0.09	0.12	0.02
10 a	14.00	14.00	—	—	0.01	0.01	—	—
30 a	4.60	4.60	—	—	—	—	—	—
	Preshower (1.7 t)				YE3 (580 t)			
1 a	24.00	24.00	8.80	8.80	0.58	0.24	0.31	0.06
10 a	7.20	7.20	1.20	1.20	0.02	0.02	—	—
30 a	2.40	2.40	0.36	0.36	—	—	—	—
	ECAL Barrel (73 t)				ME4 wall (230 t)			
1 a	5.40	5.40	1.20	1.20	0.23	0.09	0.10	0.02
10 a	0.51	0.51	0.08	0.08	0.01	0.01	—	—
30 a	0.14	0.14	0.03	0.03	—	—	—	—
	ECAL Endcap (30 t)				HF Shielding (310 t)			
1 a	45.00	45.00	11.00	11.00	66.00	32.00	35.00	7.60
10 a	4.80	4.80	0.73	0.73	2.60	2.40	0.13	0.04
30 a	1.30	1.30	0.24	0.24	0.17	0.16	0.02	0.01
	HCAL Barrel (990 t)				HF (160 t)			
1 a	1.40	0.51	0.56	0.19	910.00	430.00	470.00	110.00
10 a	0.11	0.05	0.03	0.02	35.00	30.00	1.90	0.58
30 a	0.02	0.01	—	—	1.40	1.20	0.27	0.19
	HCAL Endcap (560 t)				Thin rotating shielding (60 t)			
1 a	2.90	2.60	1.80	1.60	260.00	120.00	140.00	30.00
10 a	0.51	0.38	0.38	0.33	8.80	8.40	0.53	0.17
30 a	0.20	0.10	0.03	0.03	0.37	0.36	0.07	0.05
	Coil (440 t)				Thick rotating shielding (170 t)			
1 a	0.04	0.02	0.02	—	37.00	8.90	26.00	2.50
10 a	—	—	—	—	0.82	0.76	0.04	0.02
30 a	—	—	—	—	0.07	0.07	—	—
	YB1 (880 t)				Beam Pipe (0.2 t)			
1 a	0.01	—	—	—	4900.00	3400.00	1600.00	980.00
10 a	—	—	—	—	410.00	330.00	26.00	23.00
30 a	—	—	—	—	46.00	43.00	1.60	1.50
	η=3 shielding (150 t)				Steel nose around collimator (130 t)			
1 a	10.00	4.80	5.40	1.10	1700.00	640.00	980.00	160.00
10 a	0.55	0.50	0.03	0.01	50.00	44.00	3.80	0.86
30 a	0.08	0.08	0.01	0.01	2.00	1.80	0.45	0.28
	Endcap Yoke Nose (290 t)				Collimator (4 t)			
1 a	1.30	0.60	0.70	0.15	14000.00	14000.00	9200.00	8400.00
10 a	0.05	0.04	—	—	2700.00	2000.00	2100.00	1800.00
30 a	—	—	—	—	1100.00	560.00	160.00	140.00

Table 8: Average activities (Bq/g or γ-MeV/g/s) in various elements of CMS after 10 years of operation and the indicated cooling time. The activities in YB2 and YB3 are below 0.01 Bq/g for all considered cooling times. Values for pure high-energy (HE) activation and total activation (including neutrons) are compared. All indicated masses are estimates from the simulation.

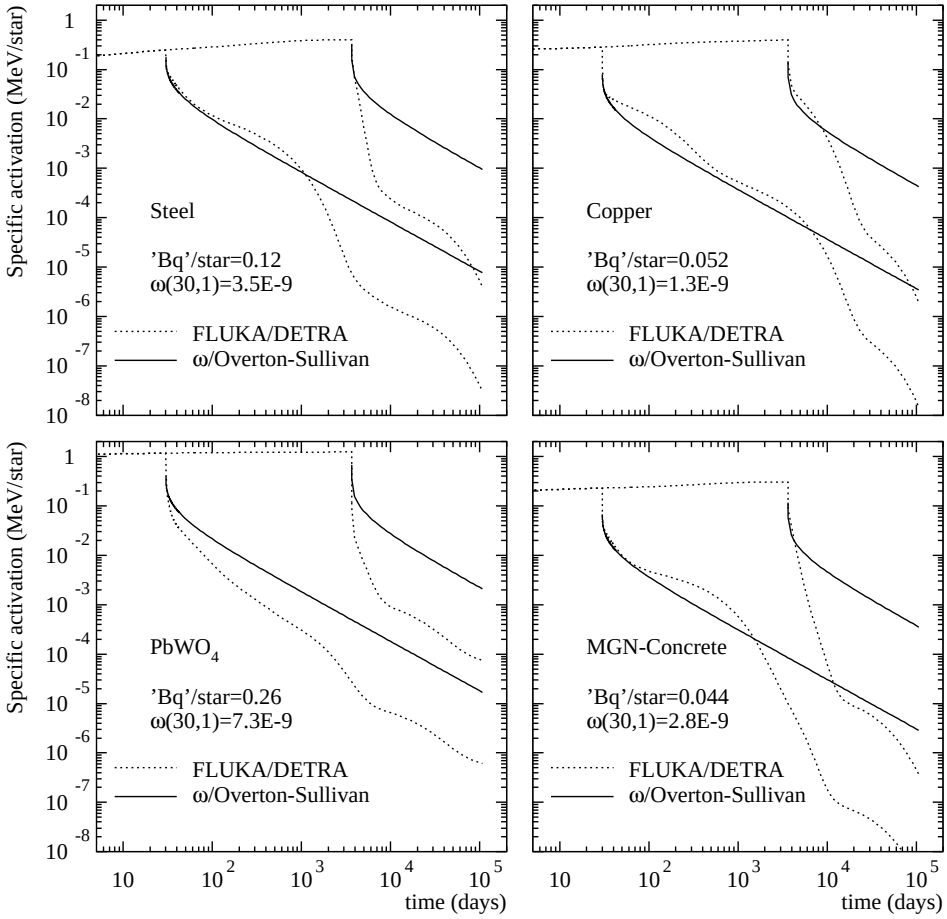

Figure 3: Comparison of FLUKA/DETRA calculations and the Overton-Sullivan time dependence for the four most important CMS materials. The absolute scaling has been obtained by fitting the $\omega(30,1)$-factors to the simulation data.

B On the ω-factors and the Overton-Sullivan formula

The presented results seem to indicate that the commonly used ω-factors and especially the Overton-Sullivan formula are not capable of giving any reasonable results. But originally Overton and Sullivan formulated their parametrization for cooling and irradiation times up to a few years and iron-like materials. With this in view a failure is not unexpected. The magnitude of the discrepancy is surprisingly large, but the formula should not be blamed for an invalid application.

In order to further clarify this issue the activation of steel, copper, $PbWO_4$ and magnetite concrete was calculated for constant irradiation of 30 days and 10 years using the radionuclide production rates obtained in the CMS simulations. The dose rate as a function of cooling time is shown in Fig. 3 together with the corresponding Overton-Sullivan prediction. The Overton-Sullivan curves have been fitted to the simulation data by fitting the 'Bq'/star factor such that the curves agree for $t_i = 30$ days, $t_c = 1$ day. The fitted values and the corresponding ω-factors (see below) are shown in the figures.

All the comparisons are fully consistent with the originally claimed validity range of the Overton-Sullivan

formula. With short irradiations the formula starts to fail after about 3-10 years of cooling. For longer irradiations the failure comes somewhat sooner (note, however, the logarithmic time axis). For $PbWO_4$, which is very far from an iron-like material, the Overton-Sullivan formula gives a too slow decay of the activity.

The relation of the 'Bq'/star factors f to the ω-factors is best established by a simple energy equilibrium argument. The ω-factors are defined as the dose in contact with a semi-infinite slab of material with uniform star density. Thus they are exactly one half of the dose inside an infinite block, where emitted and absorbed energy have to be in equilibrium. Since we have defined the 'Bq' as the emission of one 800 keV photon, each star corresponds to 800 keV of energy emitted. Thus the dose rate (Gy/h) in the active material is given as

$$D_\infty = 3600 \times 1.6 \times 10^{-10} f \frac{NE}{\rho}, \tag{3}$$

where N is the number of stars per second per cm^3, E is the energy in MeV and ρ is the density in g/cm^3.

The dose to tissue (Sv/h) in contact with a semi-infinite block is then

$$D = 0.5 \frac{\mu_{\mathrm{tiss}}}{\mu_{\mathrm{mater}}} D_\infty \approx 0.5 D_\infty. \tag{4}$$

From this we can obtain the numerical value for the ω-factor by setting N=1. For instance, using f=0.12 for iron, we get ω=3.5×10^{-9} (Sv/h)/(star/cm^3/s).

The very small ω-factor of copper, compared to steel, appears first surprising, but an inspection of the nuclide chart reveals the origin of this difference: Most spallation reactions result in nuclei just below the target, i.e. from iron manganese is produced abundantly and two significant isotopes can be identified: ^{54}Mn, ^{52}Mn. On the contrary there are no significant nickel isotopes just below copper, ^{56}Ni and ^{57}Ni require removal of several neutrons so the production cross section for them is relatively small. Therefore most of the copper activation is due to production of the cobalt isotopes ^{56}Co, ^{57}Co, ^{58}Co and ^{60}Co. But here the requirement for removal of two protons reduces the cross section.

B.1 Proposal for a new star definition

Fig. 4 shows the difference of the activation of steel in different parts of CMS. The average, used throughout this study, is shown as a solid line and can be seen to agree fairly well with the activation in the 'hottest' region just around the collimator. The activation in the outer barrel yoke YB3, however, shows a clear discrepancy from this behaviour. For short cooling times the activation per star in this well-protected region is higher than the average. For long cooling times, however, the activity drops faster.

This behaviour can be completely explained by considering the two dominating nuclei, which are ^{54}Mn for cooling times of the order of one year and ^{44}Sc for cooling times of tens to hundreds of years. These two nuclides are shown for the average steel activation, and as can be seen they are sufficient to explain most of the emitted energy at cooling times longer than a few months. This indicates that in YB3 ^{54}Mn is produced with a larger yield than around the collimator whereas production of ^{44}Ti is very small[3)]. Indeed, the production cross section of ^{54}Mn has a maximum between 30 and 50 MeV, whereas the production of ^{44}Ti requires an energy of at least a few hundred MeV. Intuitively the spectra around the collimator should be much more energetic than at YB3. This is verified by inspecting star densities with different thresholds. Around the collimator 99% of stars are created by particles above 20 MeV and 61%

[3)] Actually no ^{44}Ti was observed in the simulations for YB3, although it would have been within the statistics reach if the yield per star would have been the same as around the collimator.

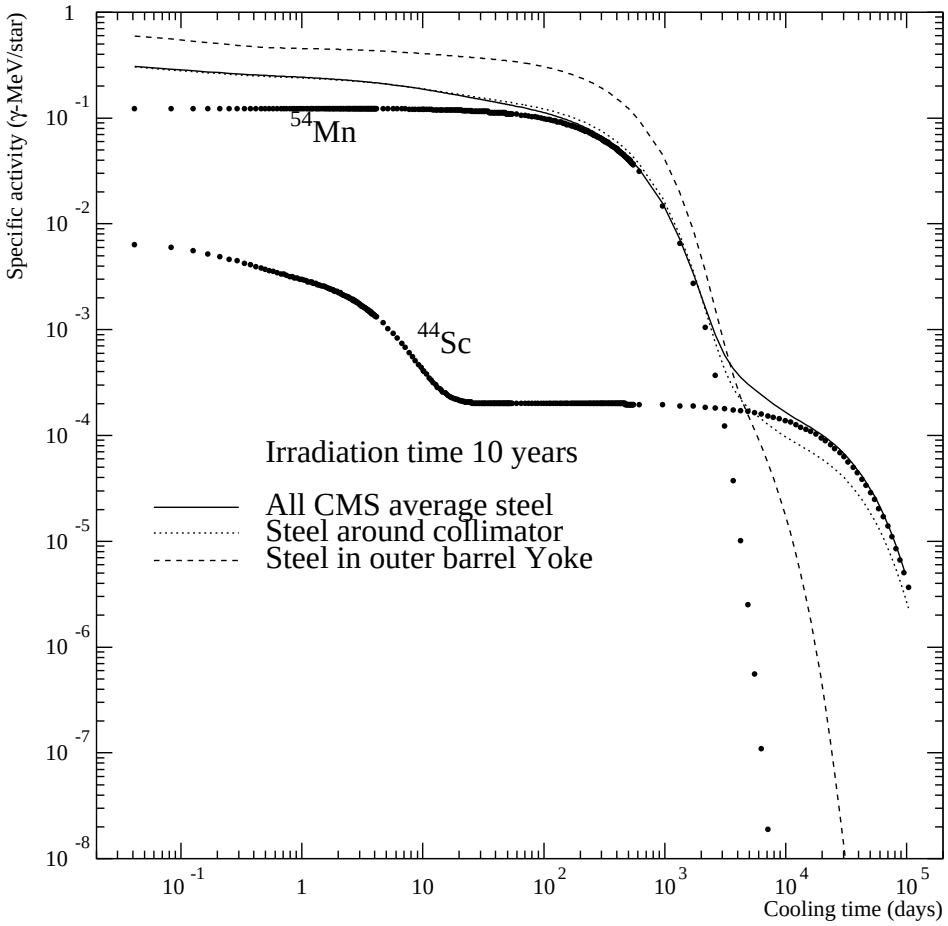

Figure 4: Induced radioactivity in steel after 10 years of irradiation. The dots show the most important nuclides and refer to the 'CMS average'. The three lines show the variation as a function of the CMS region.

by such with energy above 50 MeV. The corresponding numbers for YB3 are 98% and 26%. Thus the differences in particle spectra favour production of ^{54}Mn in YB3, but suppress the production of ^{44}Ti with respect to the collimator region. This is a striking example why the 50 MeV threshold, traditionally used in the definition of a star, should be reconsidered. Now that most of the ^{54}Mn production takes place below 50 MeV our star estimator catches only a fraction of the stars contributing to the activation. And even worse, this fraction varies with the spectrum by a factor of two. If the stars would be re-defined with a threshold of 20 MeV, this uncertainty would disappear and the spectral dependence would become much less important.

This behaviour, observed for long irradiation times, does not affect the ω-factors. If a similar comparison is done for $t_i = 30$ days all three regions coincide and agree on a unique ω-factor for steel. This is due to the simple fact that after 30 days of irradiation ^{54}Mn remains far from saturation so that other nuclides with shorter half-lifes dominate. As can be seen from Fig. 5, ^{52}Mn and ^{48}V explain most of the γ-energy emission rate after one day of cooling. Contrary to ^{54}Mn or ^{44}Ti these nuclides have rather energy-independent production cross sections.

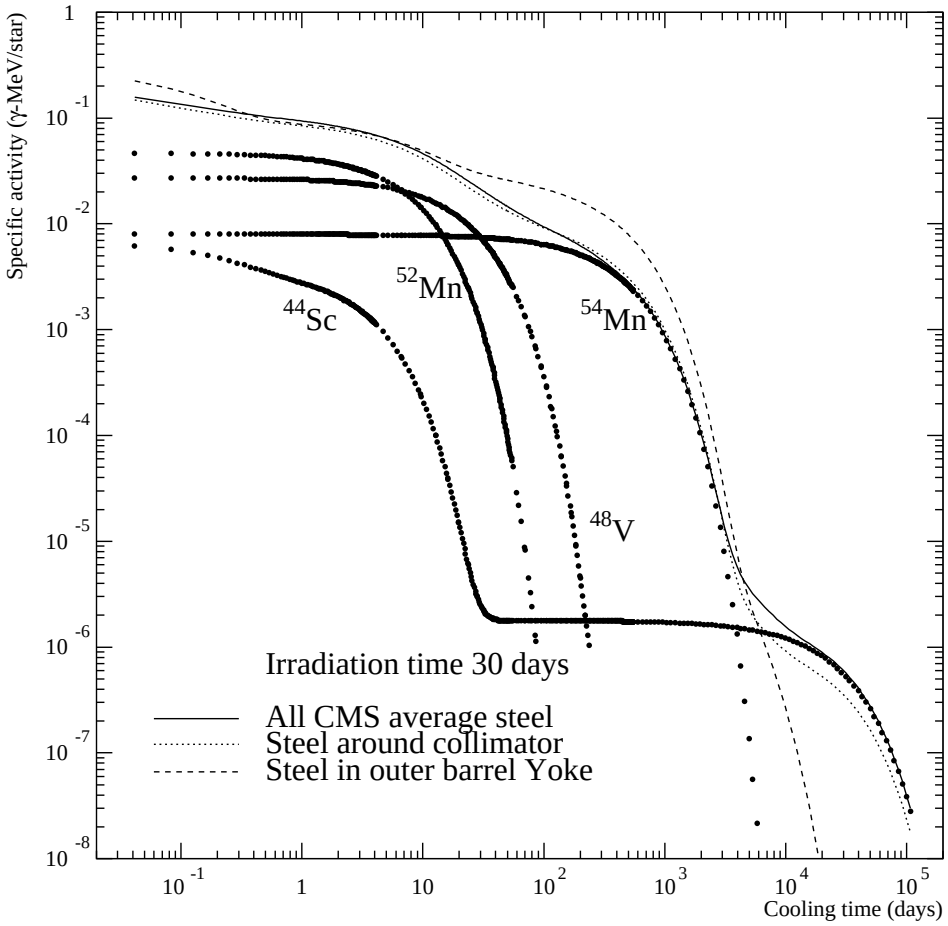

Figure 5: Induced radioactivity in steel after 30 days of irradiation. The dots show the most important nuclides and refer to the 'CMS average'. The three lines show the variation as a function of the CMS region.

Fig. 6 shows the corresponding data if stars are defined with a threshold of 20 MeV. For both irradiation times the general agreement between the different regions is improved with respect to the 50 MeV star definition. There are still discrepancies which are connected to production channels which require high threshold energies. This clearly is a spectral effect which is an inherent deficiency of the ω-factor concept and cannot be removed by any means without dropping the whole concept of assuming proportionality between inelastic interaction rate and activation.

B.2 Few warnings about ω-factors

Although the ω-factors, as derived above, appear to be on a relatively solid basis, there are a few issues which should always be remembered when applying them.

1. Since the ω-factors are defined with respect to star densities, which is a typical output from simulations codes, their numerical values are always obtained from a certain simulation code with a given threshold energy. Thus their application in connection with different codes and energy threshold

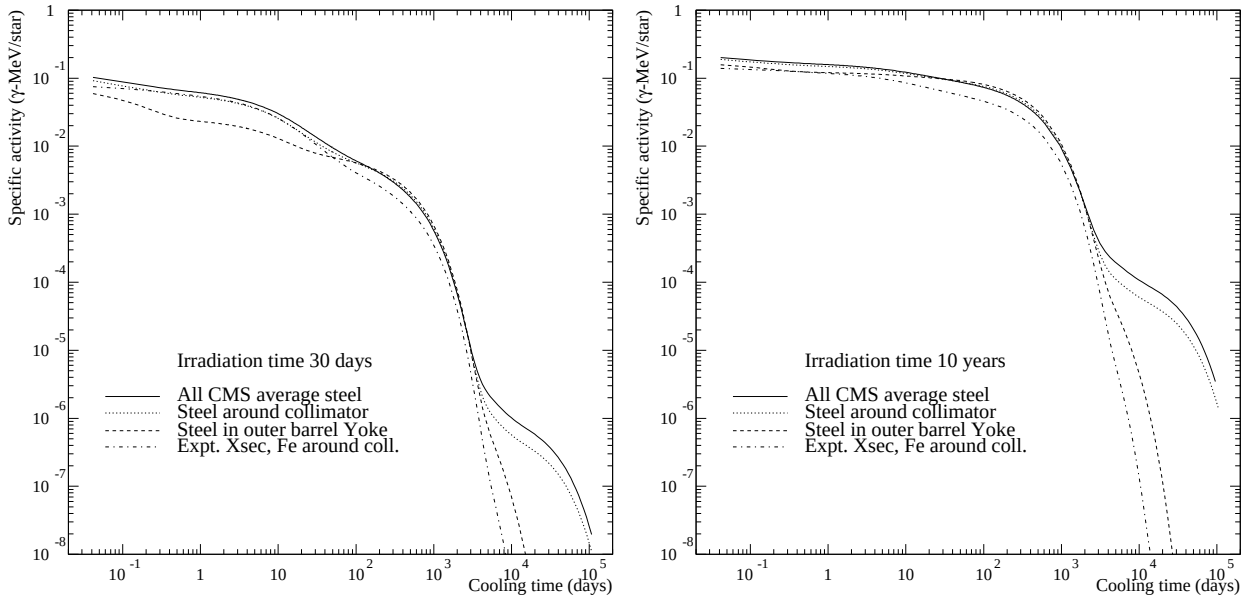

Figure 6: Induced radioactivity in steel if the star threshold is lowered from 50 MeV to 20 MeV. To be noted: the dot-dashed line with shows results based on experimental activation cross sections.

usually will lead to different dose estimates.

2. The spectral effects, discussed above, can influence the yield of individual isotopes and thus the values of ω-factors. In particular capture reactions at rest are excluded from the star definition and can cause the star-estimator to underestimate in an environment where mesons or antibaryons are present.

3. More important than the above, is the effect of neutron activation, which is not included in the ω-factors at all and can range from some 10% to dominating by orders of magnitude. How large the effect is will depend on the hadron spectrum and the irradiated material. In a homogeneous block of material where the radiation field is in equilibrium, one might consider to include the neutron activation in the ω-factors. However, in an environment like CMS, which is highly heterogeneous, such an approach is excluded and the neutron activation always has to be estimated separately. In this case the ω-factors alone can only give a lower bound on the dose rate.

C On the reliability of the radionuclide yields

Fig. 6 shows a comparison between the activation as calculated by using residual nuclei from FLUKA and by using available experimental data [5] and hadron fluxes from FLUKA [4)]. The curves for the region around the collimator (dotted and dot-dashed) are to be compared. In general we observe remarkable agreement between the two independent methods. The results using cross sections have a tendency to underestimate, which is the expected behaviour, since cross sections for some reactions just where not available and so the corresponding production is zero and not compensated by anything else. This effect

[4)] It should be emphasized that these two methods are almost independent since the hadron fluxes are very weakly linked to the microscopic model used to predict the residual nuclide yields.

becomes most obvious for cooling times in excess of 10 years, where the lack of production cross sections for ^{44}Ti causes a sudden divergence of the results. In addition a nickel content of 1% was assumed for the steel used to determine the residual nuclide yields. A corresponding assumption was not done when applying the experimental cross section where pre-evaluated data was available only for pure iron. While this small nickel content is not likely to have any effect for short t_c, it can become important for cooling times in excess of a few years.

This good agreement gives some confidence into the residual nuclide estimator, although it does not mean that individual isotope yields would be perfectly reproduced. But the residual nuclei have one advantage over experimental cross sections: if no cross section data exists for a particular reaction, it is often very difficult to figure out if this is because the cross section is small or if it is just that nobody has measured it. Thus a certain fraction of the total cross section will usually remain unknown. In the residual nuclide estimator a wrong cross section for one isotope has to be compensated in the yield of another one, since they all will automatically add up to a well known total. Since the number of different nuclides produced is often quite large, the average radionuclide yield is likely to come out fairly accurately.

In addition it must be reminded, that experimental data, even when some exist, are often very incomplete in terms of energy and projectile type coverage. Thus extrapolations in energy and scalings from one particle type to another are often needed. These procedures are likely to be much less accurate than the residual nuclide estimators.